Review

Journal of the Brazilian Chemical Society

https://dx.doi.org/10.21577/0103-5053.20240092

J. Braz. Chem. Soc. **2024**, *35*, 11, e-20240092, 1-24

Lead-Free Halide Double Perovskites Nanomaterials: Fundamentals, Recent Advances and Perspectives

Igor F. L. Ferreira,[a] *Letícia F. Magalhães,*[a] *Thaís A. S. Carvalho*[a] *and Marco A. Schiavon*[*,a]

[a]*Grupo de Pesquisa em Química de Materiais (GPQM), Departamento de Ciências Naturais (DCNat), Universidade Federal de São João del-Rei (UFSJ), Campus Dom Bosco, Praça Dom Helvécio, 74, 36301-160 São João del-Rei-MG, Brazil*

Lead-free halide double perovskites with the formula $A_2B^IB^{III}X_6$, and ordered vacancy perovskites, with the general formula $A_2B^{IV}X_6$ have recently emerged as alternative materials for advancements in lead-halide perovskites. While the main obstacles to the development of lead-halide perovskites are the use of lead and the instability of the structure, halide double perovskites allow multiple metal combinations resulting from the replacement of the lead in single perovskites by two metal-complexes or alternating vacancy metal-complexes in their crystalline structure. Although many advances have already been made in lead-free halide double perovskites, there are still some challenges to be overcome, such as the indirect and high bandgap, and the transitions prohibited by parity, which are intrinsic features of their electronic structure, and result in low energy conversion efficiency and photoluminescence quantum yields as well. Emphasizing the need to review the results of the literature so far, considering the advances and challenges presented, this work involves a systematic and embracing bibliographical research on lead-free halide double perovskites, encompassing central aspects such as their historical evolution, crystalline structure, synthesis methods, challenges faced in the field, optoelectronic properties and perspectives for the development and application of these materials.

Keywords: double perovskites, semiconductors, lead-free, halide perovskites

1. Introduction

Perovskites (PVK) correspond to a class of compounds that have a crystalline structure analogous to the mineral calcium titanate ($CaTiO_3$) and have been the subject of intense global scientific investigation in recent years.[1] The crystalline ordering of perovskites includes a wide variety of possible combinations of elements in the periodic table, existing in a diversity of subtypes, including oxides, hybrid structures (inorganic-organic), metal-free and noble gas compositions.[2-4]

One of the most used classes of perovskites in academia and industry is lead-halide perovskites. These crystals present excellent optoelectronic properties, such as narrow emission bandwidth, high absorption coefficient, remarkable carrier mobility, high photoluminescence quantum yields (50-90%), and have obtained considerable prominence in recent years, due to extraordinary developments in solar energy conversion area in a short period of time (power conversion efficiency (PCE) from 3.7% in 2009 to 25.6% in 2021).[5-8]

In addition to photovoltaic devices, halide perovskites have demonstrated advances in other optoelectronic applications, such as photocatalysis,[9,10] light-emitting diodes (LEDs),[11] and lasers.[12] This diversity of devices is made possible, in addition to the remarkable properties mentioned above, by the versatile nature of the perovskite structure, which generally corresponds to the formula ABX_3. However, there are variations in the general arrangement, which still crystallize in the perovskite structure, as is the case with halide double perovskites.[13] Halide double perovskites are crystals that feature the replacement of a divalent metal (B^{II}) by combinations of metals or metal-vacancy, in order to maintain the neutrality of the structure.[14] They are divided into two categories: conventional double perovskites, with the formula $A_2B^IB^{III}X_6$, and ordered vacancy perovskites, with the general formula $A_2B^{IV}X_6$.

*e-mail: schiavon@ufsj.edu.br
Editor handled this article: Ítalo O. Mazali (Guest)
Prof M. A. Schiavon is grateful and honored to have had Prof Oswaldo L. Alves as coauthor of many of his works in recent years.

Given the most studied perovskites so far, there are obstacles to the likely large-scale commercialization of the devices, due to the instability and toxicity of lead. The instability of lead-halide perovskite nanocrystals is related to intrinsic aspects of the material, such as the formation of secondary phases, undesirable ionic migrations and the formation of polycrystalline films, as well as external factors, such as sensitivity to environmental conditions, including humidity, oxygen, light, and heat.[5] Furthermore, lead toxicity is a critical factor, as, even at low concentrations, the metal presents a high risk to human and environmental health.[15] Among the mechanisms of action of lead in the human body, its ability to replace other divalent cations in the body, such as Ca^{2+}, is particularly relevant. This characteristic allows it to cross the blood-brain barrier, with the potential to cause serious neurological damage, especially in children.[16] The impact of extensive commercialization of these perovskites must be considered because it may increase the diffusion of lead into the environment, mainly because halides have moderate solubility in water. In a photovoltaic application, there is a risk of physical damage to the solar panels, including fires, which would contaminate the air with lead oxide.[15] These adverse factors not only emphasize the need to discuss the recycling of solar panels at the end of their useful life, but also lead to research into materials that are sustainable and free of this metal.[17]

Thus, in parallel with the research on simple perovskites, there has been a considerable increase in interest in analogous or derived structures, which have seen their greatest development in the last 5 years.[5,15] Figure 1 expresses the total number of publications in the last five years related to the term perovskite and its analogous structures, according to the Web of Science platform. The use of the term "lead-free perovskites" had a significant increase in the number of publications, also driven by advances in the area, such as the synthesis of more stable structures.

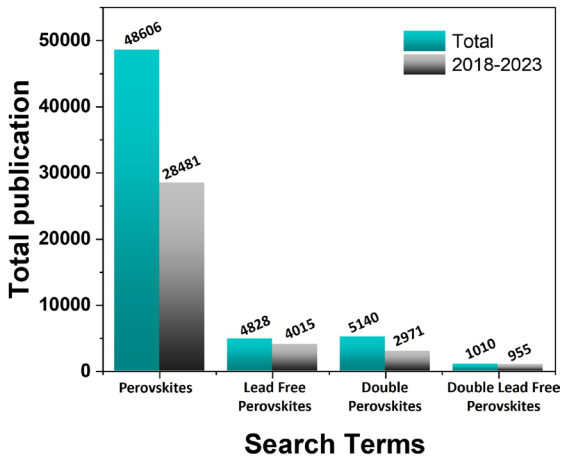

Figure 1. Bar graph relating the number of total articles published in the last five years according to the terms: "perovskites", "lead-free perovskites", "double perovskites", "double lead-free perovskites", according to the Web of Science platform.

In this sense, a series of simple perovskites reported in the literature were evaluated, using atoms close to lead in the periodic table, such as Sn, Sb and Bi.[14,18] Tin-based perovskite (Sn), for example, presents a 3D structure and a good PCE when applied to a photovoltaic device; however, the Sn^{2+} ion quickly oxidizes to Sn^{4+}.[19] Despite this, combinations of tin and germanium in organic-inorganic hybrid crystals in a photovoltaic cell were able to present a PCE of 13.24%, a record for "lead-free" materials, inspired by perovskites.[20,21]

Although there are advances, a material that exhibits properties as remarkable as lead-based crystals and that overcomes their limitations has not yet been found. Halide double perovskites were proposed as an alternative because, among some promising properties, such as stability, they offer a wide possibility of combinations in the B site, in order to present numerous structural possibilities for studies.[22] Indeed, more than 300 halide double perovskites have been synthesized, and at least twice as many structures have not yet been evaluated.[23]

Therefore, this work involves a systematic and embracing bibliographical research on lead-free halide double perovskites, encompassing central aspects such as their historical evolution, crystalline structure, synthesis methods, challenges faced in the field, optoelectronic properties and future perspectives for the development and application of these materials.

2. Brief History of Perovskites

Perovskites were discovered in 1839, when mineralogist Gustav Rose discovered a new mineral, calcium titanate ($CaTiO_3$), in a sample of skarn.[24] In 1926, with the first industrial patent related to perovskites, Victor Goldschmidt expanded the use of the term to compounds that had a structure related to this mineral.[13,24,25]

Until 1940, the commercialization of materials with the calcium titanate structure was practically limited to pigments. However, the need for new electronic technologies and ferroelectric materials with high dielectric constants during the Second World War led to the discovery of polycrystalline barium titanate ceramics, $BaTiO_3$.[24,26] This ferroelectric behavior in barium titanate arises from the dipole moment, which is related to its distorted tetragonal geometry, in which the central ion is displaced, which results in a non-centrosymmetric structure, as represented by Figure 2a. If heated above

its Curie temperature (120 °C), the structure assumes the typical cubic configuration of perovskites, Figure 2b, with the centers of positive and negative charges located at the same point, with no electric dipole, thus losing the ferroelectric character.[27] This demonstrates the correlation between magnetic properties and distortions in systems. It is worth noting that spontaneous geometry deformations occur when degenerate orbitals of nonlinear molecules subdivide in order to reduce the energy of the system.

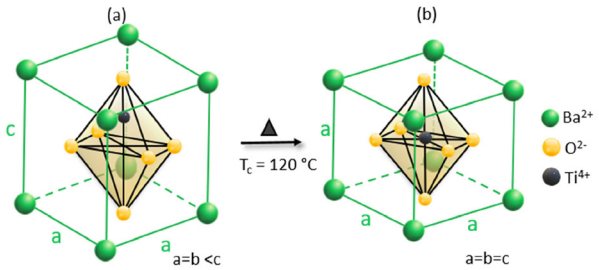

Figure 2. Representations of the (a) distorted tetragonal and (b) cubic geometries of barium titanate perovskite, $BaTiO_3$.

Throughout history to the present, oxide perovskites have been investigated with a focus on their remarkable magnetic properties, including paramagnetism, ferromagnetism and magnetoresistance capabilities.[14,21] Although they have applications in optoelectronics, it is halide perovskites that have proven to be much more suitable for this area.[21]

In the 1950s, the perovskite structure for cesium and lead halides was discovered and the optoelectronic property of photoconductivity dependent on the frequency of incident light was reported.[5,28] Advances in this area were reported in the 90s and 2000s, but it was in 2009 that the article[28] that started the well-known "perovskite fever" was published, one which has approximately 20.000 citations and marks the beginning of the drastic evolution of the energy efficiency of perovskites solar cells.[5,6] Due to their unique properties, perovskite halides have brought a new era and have emerged as a central focus of semiconductor research, and their promising optoelectronic properties are being extensively investigated.[5] A fact that can be highlighted is the example of the colloidal perovskite nanocrystals, of more than 7000 citations are presented in an article by Kovalenko's group published in 2015.[29]

3. Double Perovskites

Double perovskite oxides have been the subject of study throughout history due to their magnetic properties, similar to those of single perovskite oxides.[14,30] In current literature, these materials have also found applications in optoelectronics, presenting a PCE of 8.1% when applied to multijunction solar cells.[31] However, as previously stated, halide perovskites are still more suitable for this area of application, which motivates the search for promising properties in analogous crystalline versions, such as halide double perovskites.[22] This class has the structure of the mineral Elpasolite, K_2NaAlF_6, or the compound K_2PtCl_6.

Elpasolite was discovered in 1883 in Colorado (USA), but only in 1932, with the beginning of X-ray crystallography, its structure was elucidated.[22] In turn, the first recorded synthesis of a compound that presents this crystalline structure occurred in 1922 for $Cs_2Au^IAu^{III}Cl_6$, and, in 1938, Norman Elliott and Linus Pauling determined its structure, as well as that of the compound $Cs_2Ag^IAu^{III}Cl_6$.[32,33]

Materials with a structure analogous to the compound K_2PtCl_6, one of the first crystals with this arrangement to be structurally characterized, are halide double perovskites with ordered vacancies, also known in history as antifluorites.[22] The first recorded synthesis of these materials dates back to 1834, when Berzelius[34] reported the formation of tellurium compounds, A_2TeX_6 (wherein A = K^+, Na^+, NH_4^+, and X = Cl^-, Br^-, I^-).[22,34]

In 2014, ordered vacancy perovskites came into the spotlight due to the report by Lee *et al.*,[35] of a new class of stable iodine compounds for dye solar cell applications. The Cs_2SnI_6 crystal was used as a hole conductor in a cell with a mixture of porphyrin dyes, achieving a PCE of 8%. Recently, Kanatzidis and co-workers[36] used this perovskite as the photoactive layer for the first time, and presented a PCE of 1% and bandgap of 1.48 eV. Therefore, in subsequent years, other iodides with this structure, previously known in the literature, have been investigated again.[22]

In relation to conventional halide double perovskites, whose structure corresponds to elpasolites, a significant advance was observed at the beginning of 2016, with concomitant publications of the synthesis of cesium, silver and bismuth halides, Cs_2AgBiX_6 (X = Cl^- or Br^-), by three independent groups.[37-39] In these pioneering studies, potential properties were highlighted, such as structural stability, adjustable bandgap and low effective mass of charge carriers. As for the aforementioned research groups, the team led by Karunadasa[22,40-42] stands out, who, since then, has contributed several relevant articles on the topic.

In 2017, the formation of $Cs_2AgBiBr_6$ films, highly stable under ambient conditions, applied to a photovoltaic device, was reported, showing a promising PCE of 2.5%.[43] This result raised the interest of the scientific community, mainly due to the better stability compared to simple lead-halide perovskites.[23] The efficiency of this bromide double perovskite was developed to a record of approximately 6.4% in a study that used a hydrogen doping method in the crystalline structure.[44] Although the result is well below

those obtained by simple perovskites, this article, published in the journal *Nature Communications*,[44] presented a major advance for optoelectronics. The high indirect bandgap, which is a problem in double perovskites, has been reduced from 2.18 to 1.64 eV, which raises the theoretical Shockley-Queisser limit for single junctions from ca. 18.9% to ca. 29.8%.[44,45] However, numerical analyses of some devices using the $Cs_2AgBiBr_6$ nanocrystals as absorption layer reported PCEs values between 10.35 and 21.88%.[46]

With the development of the previously mentioned studies, since 2018, there has been a growing interest in halide double perovskite nanocrystals, mainly after the publication of independent studies on bismuth and silver halide nanocrystals, including the synthesis with iodine (Cs_2AgBiI_6), which previously was unknown experimentally.[47,48] These nanocrystals are of great interest due to their photoluminescence features, which was developed through studies with doping and metallic mixtures.[48]

Although halide double perovskite nanocrystals or nanocrystals inspired by them are still early in development and present some obstacles, such as high excitation energy, they have also demonstrated certain possibilities for future applications.[49,50] An example is in devices that use a single material capable of emitting photons from the entire visible spectrum, that is, white light emitters. Known as white light-emitting diodes, WLED, these devices are difficult to obtain, as much of the energy emitted by semiconductor nanocrystals can be absorbed by themselves or by neighboring nanocrystals, due to the small Stokes shift[51] and, therefore, represents a great challenge in current research.[50,52] Furthermore, stable double perovskite alloys, such as $Cs_2NaInCl_6$:Sb^{3+}, doped with rare earths, Sm^{3+}, Eu^{3+}, Tb^{3+} and Dy^{3+}, were also reported in the literature,[53] and presented excellent and tunable emission properties. In this case, doping with the Tb^{3+} ions achieved the highest photoluminescence quantum yield for blue light emission, of 80.1%, mainly by exerting a double effect of filling vacancy defects, as well as acting as an activator.[53]

Given that halide double perovskites are still in the early stage of development, as we can see from Figure 3, which shows the increase in publications in the area over the last five years, the focus has been on more fundamental research, such as structure assessments, the optimization of syntheses and improvement of optoelectronic properties. New combinations of metals in the B site, as well as investigations of mixing, doping and the consequences of dimensional reduction, have been reported in the literature.[22,48] Nevertheless, in addition to applications in photovoltaic cells and LEDs, the photocatalytic properties of halide double perovskites have been investigated for the production of hydrogen, for the reduction of CO_2 and for the degradation of organic pollutants, areas in which important advances have been achieved.[54-56] The use of $Cs_2AgBiBr_6$ perovskite in composites, for example, has been shown to considerably increase H_2 conversion compared to pure crystals.[54,57,58]

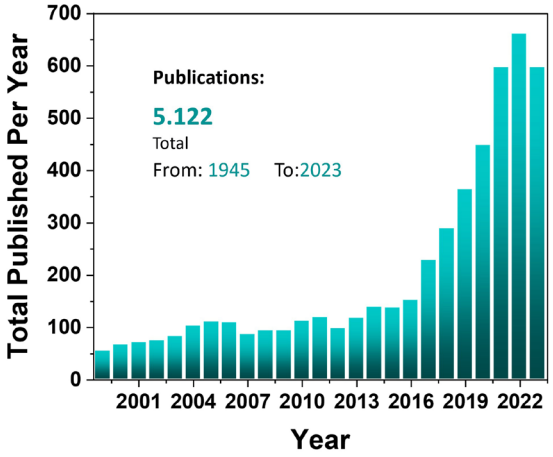

Figure 3. Record of publications of halide double perovskites by year. The insertion informs the total publications.

As previously mentioned, currently most studies still focus on understanding the features and types of halide double perovskites, such as their structure and possible variations in composition. Thus, below, we will focus on understanding these structures.

4. Structure of Perovskites

4.1. Definition

For single perovskites, the general arrangement follows the formula ABX_3, where A is generally a monovalent cation, which can be organic, such as methylammonium (MA, $CH_3NH_3^+$) and formamidinium (FA, $CH(NH_2)_2^+$), or inorganic, such as cesium (Cs^+). The B site is occupied by a divalent ion, such as Pb^{2+} or Sn^{2+}, and the X site is usually an oxide (O^{2-}) or halide ion (Cl^-, Br^- and I^-).[59] In this case, the ions from site B are coordinated by an octahedron of ions from site X, as can be seen in Figure 4.

Although the space group of greatest symmetry for perovskites is $Pm\bar{3}m$, associated with a cubic crystal system, frequent distortions in the structure result in reduced symmetry. These changes can lead to different spatial groups, finding tetragonal, rhombohedral and orthorhombic crystal systems, as shown in Figure 5.[13]

There are several materials that present variations in the general ABX_3 arrangement, but still crystallize in the perovskite structure. However, due to the importance that

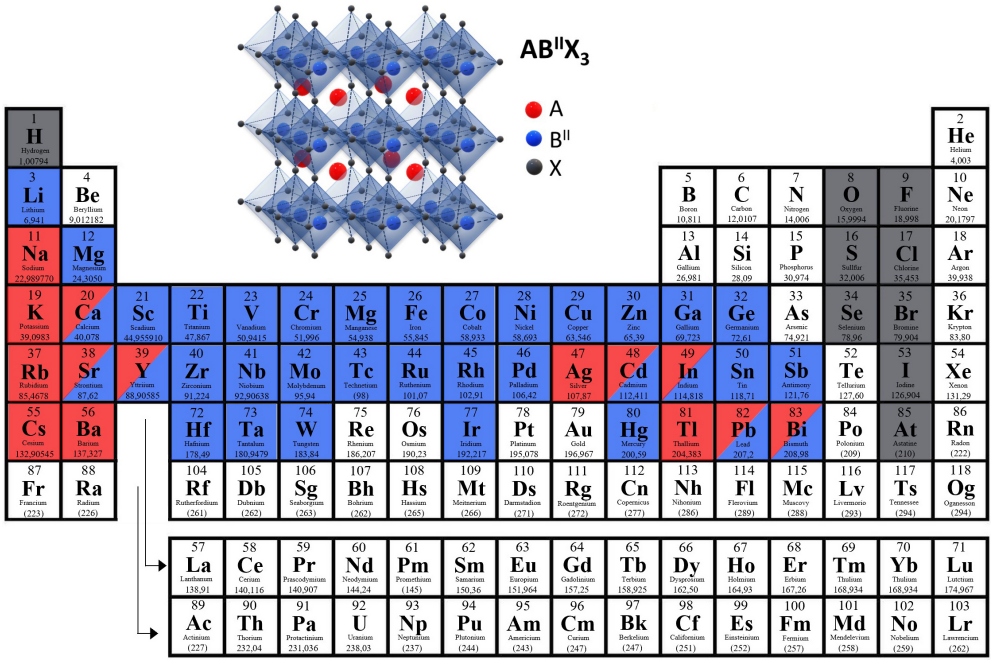

Figure 4. Illustration of the structure of a simple perovskite with possible combinations for the cations and anions of the ABX_3 arrangement.

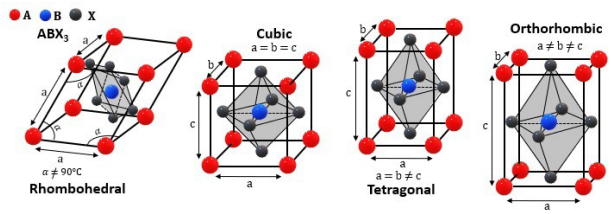

Figure 5. Representation of possible crystalline structures for the general formula of the ABX_3 perovskite as a function of distortions in the BX_6 octahedral.

perovskites have achieved in scientific world, the term has been used broadly, which may be inappropriate.[13] Although this propagation is probably inevitable, based on the articles by Akkerman[13] and Wolf,[22] and restricting the group addressed in this work to halides of metal perovskites, in addition to simple perovskites, there are anti-perovskites (A_3XY), the double perovskites, $A_2B^IB^{III}X_6$, and the double perovskites with ordered vacancies, $A_2B^{IV}X_6$.[13,22]

4.2. Double arrangement

As mentioned previously, the halides of double perovskites present a similar configuration to single perovskites, in which the difference in the arrangement is the substitution in the B site in (ABX_3), of a divalent cation (B^{II}), for combinations that neutralize the general charge of the structure.[14] For the conventional double perovskites, $A_2B^IB^{III}X_6$, the structure analogous to elpasolite is constituted by a three-dimensional pattern of alternating $[B^IX_6]^{5-}$ and $[B^{III}X_6]^{3-}$ octahedral complexes in a way that resembles the structure of rock salt (halite, NaCl).[22] Most halide compounds present, at room temperature, the cubic structure with the space group $Fm\bar{3}m$, but there are exceptions, such as the rhombohedral structure found in the $Cs_2AlBiCl_6$ crystal.[22,60]

The octahedra in conventional double perovskites are formed by central B-site cations surrounded by six halide anions, as represented in Figure 6.[14] In the interstices of this structure, there is the A cation, which is generally the Cs^+ ion. Among the main central monovalent cations (B^I) are Ag^+ and Na^+, and, for trivalent cations (B^{III}), the Bi^{3+} ion is the most used, which forms the most promising group of double perovskites in terms of optoelectronic properties and low toxicity.[23,48] However, the versatility of choosing central B-site metals is immense and researchers are in the early stages of experimenting with different combinations, such as, for example, with monovalent ions K^+, Li^+, Au^+ and trivalent In^{3+}, Fe^{3+} and Tl^{3+}.[22,48] In the case of Tl^{3+}, the compounds present good optoelectronic properties, such as a low and direct bandgap. However, their toxicity is a critical factor, and studies of thallium-based crystals are important in order to provide more fundamental understandings about the electronic effects of double perovskites.[40]

The crystallographic arrangement of the B atoms within the structure determines whether they are ordered or disordered, which plays an important role in their physical properties. Differences between ordered and disordered B sites are attributed to the size of the B cation.[61] To explain why some of the Mm^{III}, Sb^V compounds are ordered, and some are disordered. Cheetham and co-workers[62]

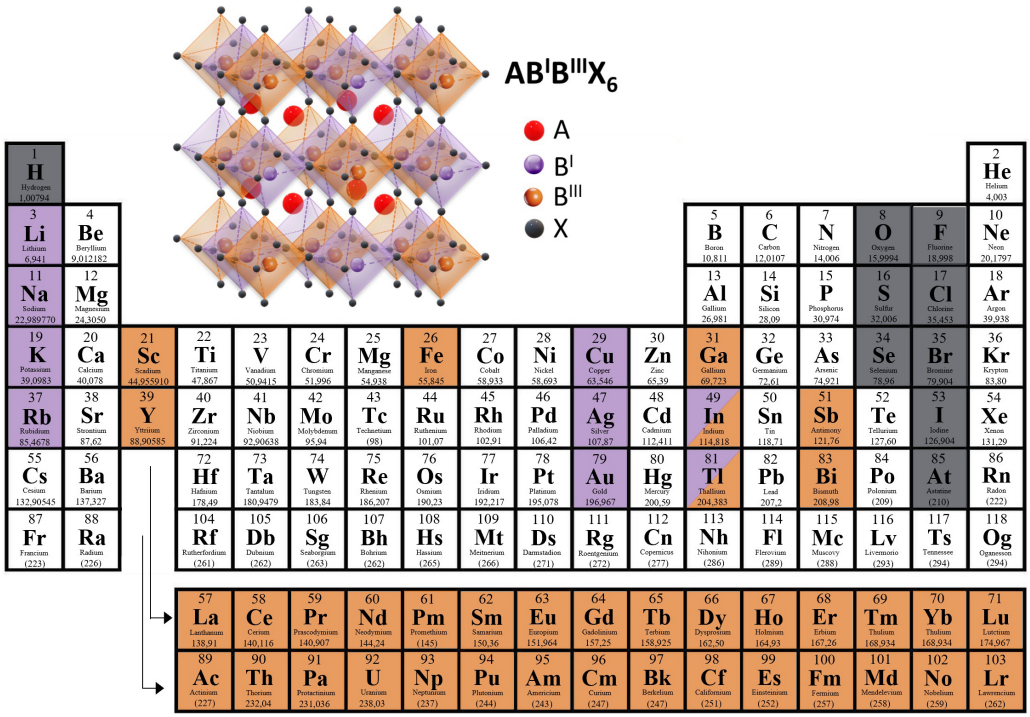

Figure 6. Illustration of the structure of a conventional double perovskite, with the $A_2B^IB^{III}X_6$, arrangement, with possible combinations for the B site cations and X anions.

demonstrated that the average (Mm^{III}, Sb^V)–X bond lengths span a bond length range ranging from 2.680 to 2.361 Å, and that the change from order to disorder occurs between 2.478 and 2.448 Å in these structures. When the octahedra [$B^{3+}X^-_6$] and [$Sb^{5+}X^-_6$] are close in size (less than 2.448 Å), no ordering is observed. The authors suggest that ordered *versus* disordered configurations of cations at site B alter the concentration dependence of electrical conductivity (σ).[61,63] This arrangement of B-site cations is considered an essential factor, as it determines the electronic properties of double halide perovskites. In recent years, most double halide perovskites reported in the literature only adopt the rock-salt ordered (0D) arrangement, mainly due to the significant charge difference between the B-site cations.[64,65] In 2021, Xiao and co-workers,[66] demonstrate that increasing the connectivity of the same octahedron, in double halide perovskites, can effectively increase electronic dimensionality and thus modulate electronic properties. In this context, double halide perovskites with columnar and layered B-site orderings should present 1D and 2D electronic dimensionalities, respectively.

The structure of halide double perovskites is highly stable, their crystal organization is thermodynamically favorable, and complete disorder is expected at high temperatures, such as 3000 K for the $Cs_2AgBiBr_6$ crystal.[67] This stability partially depends on the difference between the size of the A-site cation in relation to the underlying halides, which must be smaller. This justifies the preference for using cesium ion and the rarity of materials that contain iodine.[68,69] Nevertheless, the organization of double perovskites opens the way to a variety of stable compositions and forms, including variants with organic-inorganic hybrids.[50,70,71]

Although there are hybrid double perovskite halides, such as $MAB^IB^{III}X_6$ (MA = methylammonium; X = Cl, Br), the vast majority of materials named this way in the literature have low dimensionality (e.g., 1D, 2D), and may contain large organic chains, which do not tend to form the perovskite structure in the sense strict of the term.[13,50,69-74] For this case, the iodine structure, $MAB^IB^{III}I_6$, was reported, but it is extremely rare.[75]

Similar to single perovskites, iodine double perovskites are of great interest for the field of photovoltaics, as they are materials that can have a smaller bandgap and are more suitable for this type of application.[23,59] However, its synthesis is challenging, mainly because other crystalline arrangements tend to be more thermodynamically favorable, such as the low-dimensional phases of formula $A_3B^{III}{}_2I_9$.[23,69] Despite these obstacles, syntheses of bismuth and iodine-based compounds have been reported, Cs_2NaBiI_6 and Cs_2AgBiI_6.[47,76] There are other compounds referred to as double perovskite in the literature, with the general formula $AA'B_2X_6$ or $AA'_3B_4X_{12}$, in which metal duplicity occurs in site A, for monovalent cations. In this case, the ordering at site A requires the alloy between two cations with a large difference in ionic oxidation

rays. Typically, this ordering occurs in combination with specific octahedral rotation patterns or cation/anion/A-site vacancies.[77,78] In the literature, some examples of these perovskites which presented attractive properties are reported. For example, $CaCu_3Ti_4O_{12}$ nanocrystals (NCs) exhibited a giant dielectric effect, almost independent of temperature,[79] while $La_{2/3-x}Li_{3x}TiO_3$ possess excellent ionic conductivity.[80] The $SrCu_3Fe_4O_{12}$ NCs showed a negative thermal expansion and the $CaMnTi_2O_6$ double perovskite reveals a considerable ferroelectric polarization, in addition to a relatively high Curie temperature.[77,78,81] As they are generally oxides, considered rare and with properties similar to simple perovskites, these compounds will not be discussed in this work.[22]

4.3. Ordered vacancies

Ordered vacancy perovskite halides, with the general formula $A_2B^{IV}X_6$, belong to another subgroup of perovskites that, although historically not referred to as "double perovskites," are crystallographically identical to them.[13,22,48] Most of them, at room temperature, have the space group $Fm\bar{3}m$ and the crystalline structure of K_2PtCl_6, composed alternately of a vacancy and an octahedron with a central tetravalent cation (B^{IV}), which can be Sn^{4+}, Pd^{4+}, Pt^{4+} and Te^{4+}, as shown in Figure 7.[13]

Having a great structural similarity with the ABX_3 perovskites, the main difference is that the A_2BX_6 structure has half of the B cations absent and the rest of the B cations present form an ordered face-centered cubic arrangement. In this way, each anion becomes coordinated only to one metal B, that is, the BX_6 octahedra are no longer connected by alternating B–X bonds. As a result of this variation, the structure now presents an additional degree of freedom compared to conventional perovskites, allowing the crystal to vary the distance between the octahedra regardless of their size.[82]

Unlike conventional double perovskites, an important characteristic of these structures is their adoption of a wide range of compositions, from fluorides to iodides, without reducing symmetry and, thus, synthesis with the iodine halide is frequent, as in Cs_2SnI_6 and Cs_2TeI_6.[61] The alternating vacancies in the structure allow greater diversity of the A-site cation and greater rotational freedom for isolated $[B^{IV}X_6]^{2-}$, octahedra, and there may even be inclinations that lead to related structures, but which are not perovskites.[22] Since the octahedra are isolated, these crystals can be considered structurally 0D; however, they usually present optoelectronic properties of a three-dimensional material, as the structure is compact and these units are close to each other.[21,83]

It is worth pointing out that A_2BX_6 perovskites can be easily doped with different impurity ions, especially at the site of the tetravalent cation six-coordinated six,[84] which allows the improvement of several properties. In their studies, Zhou *et al.*,[85] demonstrated that the efficiency of the Cs_2SnI_6 perovskite in photocatalytic hydrogen production can be improved by anchoring new Pt species. Also noteworthy is

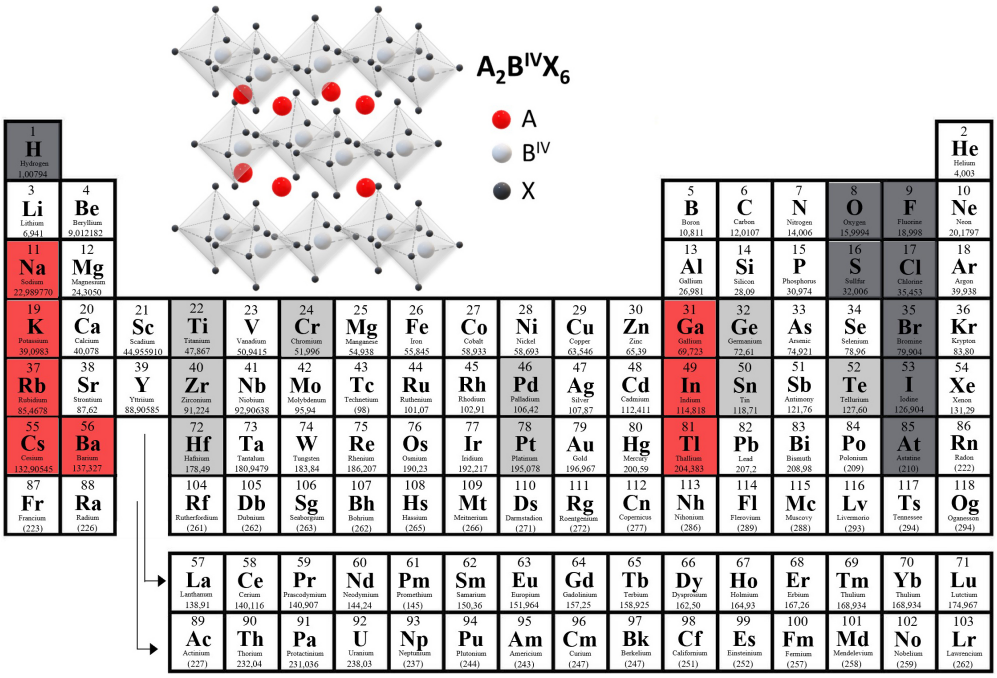

Figure 7. Illustration of the structure of a double perovskite with ordered vacancies, of arrangement $A_2B^{IV}X_6$, with possible combinations for the cations of site A, B and anions X.

the large quantity of non-toxic or low-toxic transition metals that have a stable oxidation state +4, which instigates the search for new, more favorable perovskites, which serve as replacement of toxic ions, such as Pb and Tl.[82]

In addition to this arrangement, there are perovskites formed from octahedra of trivalent metals, alternating in a 2:1 ratio in relation to the vacancies in the B sites of the crystalline structure, which have the general formula $A_3B^{III}{}_2X_9$. However, not every crystal with this formula has a perovskite structure, as is the case with $Cs_3Bi_2I_9$.[13]

4.4. Synthesis

Halide double perovskites can be synthesized in different forms, including single crystals, polycrystalline powders, colloidal nanocrystals and in thin films. Regarding the latter, the most commonly used techniques are solution deposition, such as spin coating, or vapor deposition.[86] In relation to the main methods of synthesis of crystals/nanocrystals, these include the hydrothermal method which involves precipitation induced by cooling or by anti-solvent, the hot injection technique, anion exchange reaction and synthesis by solution or in the solid state standout.[14,86,87] Most of these synthetic routes are the same as those carried out for ABX_3 perovskites.

Among the methods mentioned above, the vast majority of $A_2B^IB^{III}X_6$ NCs are produced by hot-injection (HI), which requires high temperatures, and produce, for the most part, cubic NCs.[88-90] In the synthesis of double perovskite nanocrystals, especially those made from alkali metals, it is common to use halide precursors and metal acetates, the latter being chosen due to its greater solubility in nonpolar solvents when compared to its analogous halides.[88-90]

Unlike HI, the antisolvent-induced recrystallization technique occurs at room temperature and ambient atmosphere, which makes it more economical. Furthermore, this results in the production of nanocrystals normally in a spherical shape.[88] Crystals obtained through these synthetic routes can subsequently be subjected to an anion exchange reaction, due to the high mobility of halide ions and due to the low formation energy of halide vacancies. This synthetic route is viable when dealing with metastable NCs that are difficult to be synthesized directly, such as double iodide perovskites, $A_2B^IB^{III}I_6$.[48,49]

When using these synthetic routes, it is essential to evaluate the reaction conditions to obtain quality in relation to the purity, shape and size of the NCs, which is directly related to the optical properties.[91] Thus, the temperature used, the reaction time, the stoichiometry of the reactants and the proportion of ligands must be considered. It is also necessary to evaluate which ligand is used, as the length of its chain can significantly impact the photoluminescence quantum yield (PLQY), mainly due to the fundamental role accomplished in surface chemistry, passivating the traps there.[88,92] Although oleylamine (OLA) and oleic acid (OA) are the most applied ligands to date, they are highly dynamic due to the easy proton exchange reaction between them to form the ionic ligand bond. Consequently, desorption of these ligands occurs during purification. Therefore, it becomes necessary to search for new ligands. As an example of this, we can mention the use of trioctylphosphine (TOP) together with OLA and OA to induce a stronger bond on the surface of NCs.[88,93,94]

It is also noteworthy that the colloidal stability of $A_2B^IB^{IIIX}{}_6$ NCs is lower than that of its analogous crystals, which is attributed to the greater number of surface defects generated by size reduction and dispersion solvents. That said, the study of new efficient passivation strategies is a hot topic. Among these studies, the use of shells, such as silica, in addition to doping/alloying can be effective ways to improve the stability of NCs.[88,95,96]

In general, one of the advantages of halide double perovskites lies in the fact that syntheses can be relatively simple, especially when using the solution method. However, there are techniques that require high conditions of temperature, pressure and time.[86] Furthermore, the synthesis faces limitations due to the insolubility of certain salts in organic solvents, such as silver halides, which are frequently used precursors. A common solvent used is dimethyl sulfoxide (DMSO), which tends to solubilize these salts when heated.[44] However, for the formation of high-quality films, various strategies are used, including the use of acids, such as HCl and HBr, mechanochemistry, inert atmosphere, filtration of the precursor solution and increasing the time for dissolution.[14,44,97,98]

4.5. Empirical estimation of stability

With some relationships between the ionic radii present in the ABX_3 arrangement (respectively r_A, r_B, r_X), it is possible to empirically estimate the stability of 3D perovskites, such as the Goldschmidt tolerance factor (t) (equation 1) and the octahedral factor (μ).[48,99] For double perovskites, the arithmetic mean between the ionic radii of the central metals B^I and B^{III} gives an approximation of r_B.[99]

$$t = \frac{r_A + r_X}{\sqrt{2}\left(r_B + r_X\right)} \quad (1)$$

The octahedral factor (μ) is defined as the ratio between r_B and r_X.[99] To form the stable three-dimensional structure of the perovskite, the t factor must be between 0.813 and

1.107 and the μ factor between 0.44 and 0.90.[99,100] The closer the value of t is to 1, the greater the symmetry of the ideal cubic perovskite, and the smaller μ, the more difficult the formation of the BX_6 octahedron.[48] Although some nanocrystals present crystallographic stability, thermodynamic instability is a factor that limits effective syntheses, as is the case with $Cs_2AgInBr_6$ perovskites.[101] Therefore, for the formation of perovskites, the thermodynamics of the crystals must also be evaluated, assessed by the enthalpy of chemical decomposition (ΔH_d). The chloride in double perovskites, for example, is the halide that most often form compounds with suitable t and μ. This agrees with results of enthalpy of decomposition (ΔH_d) for these compounds, which present higher values than those of other halides. Double perovskites based on bromine and iodine tend to exhibit a low, or even negative, ΔH_d, indicating that they are thermodynamically unfavorable due to favoring decomposition.[48] The factors t and μ were already studied to better explain the rarity of iodine double perovskites, including testing organic-inorganic hybrid compounds. It was mathematically demonstrated in the study that, with an increase in the halide radius, the formation of the perovskite structure decreases rapidly. However, the model used in the work generated a list of more than 300 combinations of double iodine perovskites (based on bismuth or rare earths) that have not yet been fully studied. Some examples of these double perovskites are shown in Table 1.[69,102]

Although it is widely used, the Goldschmidt factor has a limit in its applicability, especially for halides. It correctly identifies a perovskite in only 51% for chlorides, 56% for bromides and 33% for iodides. This limitation may arise from different factors, such as the significant covalent nature of the bond between the metal ion and the halide, as well as the complexity of perovskite structures. In the latter case, octahedral distortions in the sites occupied by metallic ions can be cited, which can influence the chemical and physical properties of the crystals, which are not taken into account when calculating the t factor.[103] In addition to the Goldschmidt factor, the octahedral factor can also present false positives, since the octahedra formed can refer to edge or face sharing, even if the value of μ is within the expected range for the BX_6 geometry.[104]

Due to this limitation, a new tolerance factor (τ), also dependent only on the chemical composition, was proposed (equation 2), with $r_A > r_B$ and n_A being the oxidation number of the cation at site A. A value of the factor τ less than 4.18 indicates the formation of perovskite.[104]

$$\tau = \frac{r_x}{r_B} - n_A \left(n_A - \frac{r_A / r_B}{\ln\left(r_A / r_B\right)} \right) \quad (2)$$

Table 1. Double perovskites with their respective tolerance and octahedral factors[102]

Perovskite	Tolerance factor	Octahedral factor
$Cs_2CuInCl_6$	1	0.43
$Rb_2CuInCl_6$	0.96	0.43
$K_2CuInCl_6$	0.93	0.43
$Cs_2NaInCl_6$	0.96	0.5
$Cs_2AgInBr_6$	0.93	0.49
$Cs_2AgInCl_6$	0.94	0.54
$Rb_2AgInCl_6$	0.89	0.54
$K_2AgInCl_6$	0.87	0.54
Cs_2KInCl_6	0.84	0.67
Cs_2LiYCl_6	0.97	0.45
$Cs_2LiCeCl_6$	0.96	0.48
$Cs_2NaTbCl_6$	0.94	0.54
$Cs_2NaCeCl_6$	0.92	0.56
$Cs_2NaEuCl_6$	0.89	0.6
$Cs_2NaSbCl_6$	0.96	0.49
$Cs_2AgSbCl_6$	0.94	0.53
$Cs_2AgSbBr_6$	0.93	0.48
Cs_2KSbCl_6	0.87	0.66
$Cs_2NaBiCl_6$	0.92	0.56
$Cs_2AgBiCl_6$	0.9	0.6
$Cs_2AgBiCl_6$	0.9	0.6
$Cs_2AgBiBr_6$	0.89	0.55
Cs_2KBiCl_6	0.73	0.83

With this calculation, the accuracy increases to ≥ 90% for halides. Furthermore, when using Platt sizing, a probabilistic quantity is obtained, in which, as τ decreases, the probability of the material being stable in the perovskite structure increases. Thus, using τ, it was possible to estimate 23,314 new double perovskite structures, considering oxides and halides.[104]

With the stability defined, it is possible to distinguish the different crystalline systems formed by double perovskites by calculating the suitability factor (ϕ), identified in equation 3.

$$\phi = \sqrt{2\frac{r_A}{\left(r_B + r_X\right)}} \quad (3)$$

In this case, when $\phi > 1$ the formation of cubic crystals occurs, when the suitability factor is equivalent to $0.93 < \phi < 1$ the tetragonal crystal system is formed, while orthorhombic crystals occur with $0.90 < \phi < 0.93$ and $\phi < 0.93$ indicates the monocyclic crystal system.[78]

Specifically dealing with ordered double vacancy perovskites, crystallographic stability is influenced by

temperature, which leads to possible phase transitions. An example of this was exposed by Boysen and Heat[105] for K_2SnCl_6, which presented t equal to 0.9023 and μ equal to 0.3812 at room temperature, indicating the formation of the cubic crystal system belonging to the space group Fm3m. However, when it is cooled, due to rotations of the Cl_6 octahedron, it reorganizes into the tetragonal system at 265 K and, at 190 K, into the monocyclic structure.[106]

4.6. Optoelectronic properties

In addition to stability, due to the number of possible combinations in double perovskites, there is greater versatility in modulating optoelectronic properties compared to single perovskites. However, these properties are still significantly inferior.[22] Among the main limitations of double perovskites those that stand out are the indirect and high bandgap (> 2 eV), parity-forbidden transitions, low photoluminescence quantum yield, low electronic dimensionality, low mobility and low charge lifetime.[14,23,40,107]

Bismuth-based compounds, for example, constitute the most explored and promising group of double perovskites.[14,23] Double perovskite NCs (Ag^+Bi^{3+}) exhibit prominent sub-bandgap absorption, mainly corresponding to indirect transitions, which is related to surface defects, thus leading to low PLQY.[108] Two strategies to improve yield would be to increase the rate of radiative recombination and reduce the rate of non-radiative recombination.[52] Yang *et al*.[109] demonstrate that sub-bandgap trap states can cause radiative and non-radiative recombination in this nanocrystal. The capture process can be passivated by the OA ligand, and the key measure to further improve PL is to further decrease surface defects.[109] As mentioned, the record PCE is approximately 6.4% for $Cs_2AgBiBr_6$.[44] This result was achieved due to the improvement in film quality, mobility and lifetime of charges, provided by hydrogen doping in the interstices of the network. In addition to doping, techniques such as mixing and changing dimensionality are also studied with the aim of overcoming the associated challenges.[14,110]

4.7. Electronic structure

Part of the superiority of lead-based perovskites comes from the electronic configuration of this metal: $[Xe]6s^24f^{14}5d^{10}6p^0$.[111] Electronic transitions in the perovskite bandgap generally do not directly involve the A-site cation and occur in the $[PbX_6]^{4-}$ octahedral complex, in which the p^6 orbitals of the halide, juxtaposed to the $6s^2$ orbitals of lead, form the maximum of the valence band (MVB). The empty $6p^0$ orbitals of Pb^{2+} constitute the conduction band minimum (MCB).[14,48] The MVB in this material is dominated by the character of the p^6 orbital of the halide; therefore, electronic transitions occur from ligand to metal. This transition is also observed in perovskites with vacancies, $A_2B^{IV}X_6$, since, generally, there is no metal with an orbital energy close to MBV, thus exhibiting a purely halide character.[22,42]

In contrast, in conventional double perovskites, $A_2B^IB^{III}X_6$, the electronic structure is considerably more complex, and the character of the MVB is variable, often influenced by one of the B-site metals.[112] In this context, the electronic transition occurs, in general, from metal to metal. For this reason, the electronic structure becomes dependent on the compatibility between the s orbitals of the B site ions, that is, on isoelectronic configurations.[22,42] Bi^{3+}, for example, has a filled external s orbital ($6s^2$), when combined with an ion such as Ag^+, which has a free s orbital ($5s^0$), it tends to form an indirect bandgap compound; however, combined with Tl^+ ($6s^2$) the bandgap is generally straight. While the In^{3+} ($5s^0$) or Tl^{3+} ($6s^0$) ions in combination with Ag^+ ($5s^0$) form a compound with a direct bandgap.[42,48,113] However, compounds with In^{3+} ions are usually unstable, due to the tendency of In^+ to oxidize to In^{3+} [114] and compounds with Tl^+/Tl^{3+} are toxic, which is why most of the stable conventional double perovskites studied present an indirect bandgap, a characteristic that is one of the main limitations of these compounds.[42]

4.8. The size and nature of the bandgap

The indirect and high bandgap of double perovskites represents one of the challenges to be overcome, especially for application in photovoltaic devices. According to the Shockley-Queisser Limit, the ideal forward bandgap for a single-junction solar cell lies between 1.10 and 1.40 eV.[23,45] Curiously, the stable cubic structure of double perovskites may be responsible for the high bandgap value, due to the restriction of interactions between orbitals that decrease the energy value of the conduction band.[14]

As previously mentioned, iodine tends to form compounds with smaller bandgaps, compared to other halides and, for conventional double perovskites, such structures are thermodynamically unfavorable, which makes their synthesis rare. Therefore, it is of interest to researchers to develop strategies to reduce the bandgap in chlorides and bromides. Ji *et al*.,[115] for example, obtained the lowest value (1.72 eV) for the $Cs_2AgBiBr_6$ perovskite, controlling the temperature and crystal growth speed. Furthermore, it is worth mentioning that the lowest bandgap value (0.95 eV) found in perovskite halides was for the

$Cs_2AgTlBr_6$, crystal, although this should not be used in devices due to thallium toxicity.[40]

Regarding the indirect nature of the bandgap, referring to the asymmetry between the MVB and the MCB, greater difficulties arise for the synthesis of high quality crystals, since the material needs to be thicker to increase the probability of absorption, thus representing a big challenge.[22] This need arises from the fact that, in these types of semiconductors, optical electronic transitions depend, in addition to the absorption of a photon, on the change in electron momentum mediated by a phonon (vibration of the crystal lattice), which decreases absorption efficiency.[113] Although ordered vacancy perovskites often do not present this problem, their applications are limited due to the high concentration of vacancies.[13]

The presence of an indirect bandgap in a material does not necessarily disqualify it for photovoltaic applications. In fact, crystalline silicon, which predominates as the main material commercially used in solar panels around the world, has this characteristic.[116] It is common for crystals with an indirect bandgap to have a high lifetime for the recombination of charge carriers, which reduces energy loss and mitigates the effects of thickness.[39] Exceptionally high lifetimes have been reported in the literature for $Cs_2AgBiBr_6$ single crystals (E_g = 2.19 eV), with values of approximately 660 ns and up to 1.4 µs.[39,117]

However, it is important to highlight that morphology significantly impacts optoelectronic properties, especially in conventional double perovskites. Imperfections in the structure lead to a high rate of traps on the surface of these crystals which, although of low energy, if they were passivated, would improve the diffusion distance of charges.[44,113] Some examples of bandgap values can be seen in the tables available in the Applications section.

4.9. Transitions prohibited by parity

In perovskites, there are also parity-forbidden transitions, which can considerably affect optoelectronic properties, especially in double perovskites.[118] Due to the existing octahedral complexes, according to Laporte's selection rule for centrosymmetric compounds, the permitted transitions between orbitals must occur with a change in parity, g (gerade) ↔ u (ungerade), which implies a change in the azimuthal quantum number (l) (s ↔ p, p ↔ d and d ↔ f).[119] However, due to the asymmetries in the octahedron, whether intrinsic to the structure or imposed by the environment, the Laporte restriction is relaxed. Thus, forbidden transitions occur that can influence the value of the optical bandgap and decrease absorption.[48,113,118,119]

That way, even if a direct and low bandgap is achieved in double perovskites, the crystal may not be suitable for certain optoelectronic applications. Meng *et al.*[118] examined the effects of parity-forbidden transitions in different double perovskites. Of the six types of crystals with direct bandgap, only those that contained the metals In^+ and Tl^+ in the B^I site and Sb^{3+} and Bi^{3+} in the B^{III} site exhibited robust electronic transitions. Furthermore, most structures containing alkali metals showed a direct bandgap, but with transitions that were weak or strictly prohibited by parities.

However, if the regions of parity-forbidden transitions are narrow and close to the edges of the conduction and valence bands, this may be a favorable characteristic for a device.[22] This property can extend the lifetime for charge carrier recombination while not significantly affecting optical absorption due to a lower probability of forbidden transitions, as reported by Karunadasa's group for the Cs_2AgTlX_6 (X = Cl, Br) crystal.[40,113]

Although this property may be beneficial in certain cases, it is essential to develop strategies to manipulate the electronic structure in order to minimize parity-forbidden transitions. One of the properties affected by such transitions is the photoluminescence quantum yield. Thus, studies have investigated techniques such as doping and mixing metals, which have demonstrated the potential to break the inversion symmetry of octahedra.[48,52,120]

4.10. Perovskites alloys

One of the advantages currently explored in double perovskites is the stable adhesion of impurities to the crystals, either as a perovskite alloy or through doping, to enhance optoelectronic properties.[48] Although it is another concept used comprehensively, according to the definition of Weller *et al.*,[119] when the replacement of atoms occurs in the range of 0.1 to 5%, which maintains the crystalline structure unchanged, the technique is specified as doping.

The inclusion of impurities can be isovalent (of the same valence) or aliovalent, which often generates vacancies.[22] When a metal of the same valence is added to a perovskite, a change in the size of the bandgap is expected, but not in its nature. It has been reported, for example, that as the relative concentration of the Sb^{3+} cation, isovalent to bismuth, increases in the $Cs_2Ag(Bi_{1-x}Sb_x)Br_6$ perovskite alloy, the bandgap tends to decrease. This is because, due to relativistic effects, the 5s orbital of antimony has higher energy than the 6s orbital of bismuth.[22,121] However, when dealing with the inclusion of aliovalent metals, changes in the nature (size and symmetry of the bandgap) are expected.[22]

Double perovskite alloys are generally synthesized by incorporating isovalent metals into the B site, although they can also occur in the A site, as well as in conjunction with doping.[22,110,122] Such techniques form complex systems and demonstrate the versatility of these materials, such as the replacement of Bi^{3+} ions by In^{3+}, associated with the doping of Mn^{2+} in the $Cs_2Na(Bi_{1-x}In_x)Cl_6$ crystal.[110] This synthesis results in an intense orange emission, whose color range, as well as the size and nature of the bandgap, can be adjusted according to the relative concentration of the ions. Furthermore, alloy combinations are also carried out in ordered vacancy perovskites, such as the insertion of Cs^+ in the Rb_2HfCl_6 crystal doped with Bi^{3+}, which results in a progressive increase in light emission (ca. 0 to 66%).[122]

Several ions have been used in doping and alloying techniques, in addition to the H^+, Mn^{2+} and Bi^{3+} mentioned, cations such as Cu^+, Al^{3+} and rare earths are also used.[53,123,124] Table 2 summarizes some of the main elements used in the doping processes and formation of double perovskite alloys to modulate their optoelectronic properties, as well as the synthesis methods.

Recently, copper insertions into double perovskite crystals have been reported, resulting in darkening, a potential indicative of improvement in optoelectronic properties.[23,98,123,125] In fact, these studies observed a decrease in the bandgap for the $Cs_2AgInCl_6$ crystal and the appearance of a strong near-infrared absorption for the $Cs_2AgBiBr_6$ crystal. The change in crystal tone to black, frequently reported in the literature, is attributed to the extension of the spectral absorption region. This amplification usually leads to a decrease in the bandgap and can be induced both by doping processes and by crystal growth control methods.[40,115] Figure 8 exemplifies the change in tone following the addition of Fe^{3+} ions to the $Cs_2AgInCl_6$ material.

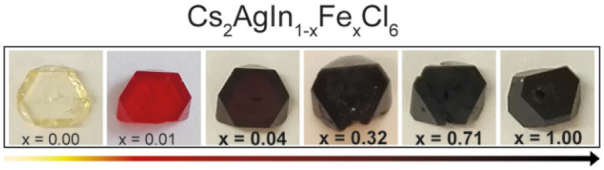

Figure 8. Change in hue of a double perovskite single crystal as a function of molar ratio between B^{III} site metals (reproduced from reference 126 with copyright permission 2021 from Royal Society of Chemistry).

Regarding the use of rare earths, such as La^{3+}, Sm^{3+}, Eu^{3+}, Yb^{3+}, doping is attractive for LED applications due to the unique luminescent properties of these elements.[98,120,127] Wang and co-workers[52] performed a co-doping with Eu^{3+} and Sb^{3+} in an yttrium-based single crystal, Cs_2NaYCl_6, achieving a photoluminescence quantum yield of 58%, the highest among red double perovskites.[127] In the case of devices, an excellent photoluminescence yield result for white light LEDs is approximately 86%, achieved in 2018 with the mixture of Na^+ in the B^I site of the $Cs_2AgInCl_6$ crystal, together with Bi^{3+} doping.

Furthermore, alloying and doping have also contributed to advances in double perovskite nanocrystals. However, while single perovskite colloidal nanocrystals are considered one of the most promising materials, the field of double perovskites still needs further development. The stability and luminescent properties of these structures are still inferior to those of simple perovskites and their bulk versions.[48]

4.11. Dimensionality

Dimensional reduction is currently one of the most investigated strategies for simple perovskites, which are commonly applied in 3D form. This is due to increased chemical, thermal stability and moisture resistance, which constitute some of its main problems.[128,129] Generally, the reduction in dimensionality to the 2D or 0D form occurs with the insertion of large hydrophobic organic cations between the layers of the BX_6 octahedral complex, which are stabilized by intrasurface van der Waals interactions.[128,129]

The critical issue in hybrid 2D "perovskites" lies in their high bandgap, partially due to the high binding energies of the excitons, which impacts, for example, on PCEs in photovoltaic applications.[128,129] However, dimensional reduction is a technique that is beginning to show very significant results for simple perovskites in the photovoltaic area, reaching a certified PCE of 18.0 (± 0.3)% for the structure (butyldiammonium)$(Cs_{0.1}FA_{0.9})_4Pb_5I_{16}$, in 2D dimensionality, obtained by solvent vapor annealing.[130]

Regarding double perovskites, dimensionality reduction is a fairly recent technique, and most reported two-dimensional compositions do not have three-dimensional analogues. This is due to the greater structural flexibility in low-dimensional crystals, which also significantly alters their properties.[22,41] Calculations indicate that it is possible to modify the bandgap symmetry, probably due to the confinement effect.[41] In the future, dimensional reduction may bring improvements to properties by solving problems in electronic structure.[14] However, currently, the optoelectronic properties of these crystals are considerably inferior to those of their three-dimensional versions, due to this flexibility and the confinement effect.[22,23] Therefore, one of the strategies used to improve PCE in photovoltaic applications is the use of 2D/3D hybrid systems, such as $Cs_2AgBiBr_6/(PEA)_4AgBiBr_8$ (PEA = phenethylammonium) crystals. Nevertheless, the efficiency is still very low, standing at 2.5%.[131]

Table 2. Double perovskite alloys and doping: ions, morphology, and synthesis methods

Perovskite	Inserted elements	Synthesis method	Morphology	Max PLQY / %	Applications	Reference
$Cs_2AgInCl_6$	Na^+, Bi^{3+}	hot injection	nanocrystals	22	[a]	96
$Cs_2NaInCl_6$	Bi^{3+}, Mn^{2+}	hydrothermal	single crystal	56	[a]	82
$Cs_2NaInCl_6$	Ag^+	hot injection	nanocrystals	31.1	[a]	97
$Cs_2AgBiBr_6$	Yb^{3+}, Eu^{3+}	hydrothermal, antisolvent	bulk powder, thin film	–	[a]	98
$Cs_2AgInCl_6$	Na^+, Bi^{3+}	hydrothermal	single crystal	–	scintillator for X-ray imaging	99
$Cs_2NaInCl_6$	K^+, Sb^{3+}	solution (HCl)	single crystal, bulk powder	82	[a]	100
Cs_2KInCl_6	Na^+, Sb^{3+}	solution (HCl)	bulk powder	93	[a]	100
$Cs_2AgBiBr_6$	Cu^+	hydrothermal	single crystal	–	potential application in near-infrared photodetectors	94
$Cs_2AgInCl_6$	Cu^+	hot injection, solution (HCl)	nanocrystals, bulk powder	–	potential application in solar cells and other optoelectronic devices	77
$Cs_2LiBiCl6$	Mn^{2+}	solid state	bulk powder	–	[a]	101
$Cs2NaBiCl_6$	Mn^{2+}	solid state	bulk powder	–	[a]	101
$Cs_2AgInCl_6$	Cu^+	hot injection	nanocrystals	–	potential application in solar cells and other optoelectronic devices	102
$Cs2AgBiBr_6$	H^+	solution, spin coating	thin film	–	solar cell	46
$Cs_2AgBiCl_6$	Al^{3+}	hot injection	nanocrystals	17.2	LED	95
$Cs_2AgBiBr_6$	Sb^+	hydrothermal	bulk powder	–	composite to enhance photocatalytic oxidation of toluene	56
$Cs_2NaInCl_6$	Sb^{3+}, Sm^{3+}, Eu^{3+}, Tb^{3+}, Dy^{3+}	hot injection	nanocrystals	80.1	anti-counterfeiting devices, optical and LED thermometry	53
Cs_2NaYCl_6	Sb^{3+}, Eu^{3+}, Tb^{3+}	hydrothermal	single crystal	58.3	LED	103
$Cs_2AgInCl_6$	K^+, La^{3+}	hydrothermal	bulk powder	19.9	LED	104
$Cs_2NaBiCl_6$	Mn^{2+}	solution (HCl)	bulk powder	–	[a]	105
$Cs_2AgInCl_6$	Sb^{3+}, Yb^{3+}	solution (HCl)	bulk powder	50	LED	91
$Cs_2AgInCl_6$	Fe^{3+}	hydrothermal	single crystal	–	potential application in solar cells and other optoelectronic devices	106
Cs_2SnCl_6	Mn^{2+}	hot injection	nanocrystals	–	[a]	107
Rb_2ZrCl_6	Cs^+, Te^{4+}, Sn^{4+}	hydrothermal	bulk powder	69.7	LED	108
Cs_2HfCl_6	Sb^{3+}, Pr^{3+}, Eu^{3+}, Tb^{3+}, Ho^{3+}	hot injection	nanocrystals	40.7	scintillator for X-ray and LED imaging	109
Cs_2SnCl_6	Te^{4+}, Bi^{3+}	solution (HCl)	bulk powder	38.6	LED	110
Cs_2SnCl_6	Bi^{3+}	hot injection	nanocrystals	35.2	[a]	111
Cs_2ZrCl_6	Te^{4+}, Er^{3+}, Nd^{3+}, Yb^{3+}	co-precipitation	bulk powder	6.1	[a]	112
Rb_2HfCl_6	Cs^+, Bi^{3+}	solution (HCl)	bulk powder	66	[a]	93
Cs_2SnCl_6	Gd^{3+}	hydrothermal (solvothermal)	bulk powder	–	[a]	113
Cs_2SnCl_6	La^{3+}	hydrothermal (solvothermal)	bulk powder	55	[a]	114

[a]No application. PLQY: photoluminescence quantum yield; LED: light-emitting diode.

5. Applications

The imminent optoelectronic applications of double perovskites increasingly attract the attention of scientists to understand their electronic properties and phase transitions. Although related studies are still in the initial phases,

that is, in the search for greater understanding related to fundamentals and properties, there are already some reports on applications in solar cells, photocatalysts, LEDs, among other areas.

5.1. Solar cells

Perovskites feature tunable optical and electronic parameters, which are attractive for energy-related applications. This fact has attracted a lot of attention in recent years, achieving considerable progress that has allowed a rapid advance in PCE above 20%. However, limited electrical conduction, toxic nature and long-term instability restrict the wide use of these materials.[132,133]

Thus, research was extended to overcome these challenges, drawing attention to other structures with the replacement of lead, Pb, with other non-toxic elements, such as bismuth, Bi. Despite the possible substitution, the Bi^{3+} cation ends up forming a 0D or 2D structure in the $A_3B_2X_9$ structure, as it does not support the 3D structure of traditional perovskites, ABX_3. However, this formed structure leads to low performance of photovoltaic devices due to low charge mobility, high exciton binding energy, high density of trap states and short carrier diffusion length.[132]

In view of this, in order to maintain the 3D structure, the use of $A_2B^{I}B^{III}X_6$ double perovskites as potential light-absorbing materials is investigated, which preserves the total number of valence electrons in the unit cell unchanged in relation to traditional perovskites.[132] Among this class of double PVK, the compound $Cs_2AgBiBr_6$ has been, to date, the most investigated as a light-harvesting material for photovoltaic devices. However, development is still in the early stages, with performance affected by severe hysteresis, thus presenting PCEs below 3% and low photocurrent densities.[48,134]

Aiming to improve the performance of these perovskite solar cells (PSC) based on $Cs_2AgBiBr_6$, modifications in the thin film deposition techniques are investigated, as well as variations in the composition and structure of the devices.[134] Another possibility is to expand the absorption range, which can be achieved by using dyes acting as co-sensitizers. Wang *et al*.[135] manufactured $Cs_2AgBiBr_6$ PSC hybridized with three indoline dyes: D102, D131 and D149, achieving, for the latter, a PCE of 4.23%. Shao and co-workers[136] presented a PCE of 2.84% after reporting the introduction of the dye N719 as an intermediate layer, which not only expanded the absorption range, but also suppressed the recombination of charge carriers, accelerated the extraction of holes, built an appropriate power level and greatly increased the stability of PCSs under environmental conditions.

Among the research already carried out, the highest PCE obtained for solar cells based on $Cs_2AgBiBr_6$ was 6.27%, achieved through a hydrogenation method, which allowed a reduction in the material's bandgap from 2.14 to 1.61 eV. Furthermore, the study observed remarkable stability in nitrogen environments under light illumination, both at room temperature and at temperatures as high as 85°C.[44]

Some ordered double vacancy perovskites, A_2BX_6, based on halides are considered promising candidates for various optoelectronic devices. An advantage is that the choice of atoms with different ionic radii can adjust the structural composition, influencing and optimizing various physical properties of the material, such as bandgap, magnoelectronic and spintronic memory.[133]

Most studies related to these perovskites for application in solar cells were carried out through theoretical calculations, with few cases of experimental tests. For example, Mahmood *et al*.,[133] performed density functional theory (DFT) calculations of the Rb_2PtCl_6 and Rb_2PtBr_6, structures, finding direct bandgap intervals of 2.62 and 2.1 eV, respectively. The perspective of energy-related applications was due to the bandgap located in the visible energy range, in which they found a maximum absorption in the range of 2.5-4.0 eV, with minimum optical loss, and due to their stable cubic structures. In another study carried out by Othman Hakami,[137] using DFT, the compounds A_2ZrI_6 (A = Ga, In, Tl) were systematically investigated regarding their optical, electronic and thermoelectric properties, aiming for applications in solar cells. They determined a direct bandgap, which increases from 2.25 to 2.28 eV, and 2.37 eV by replacing Ga with In and Tl, in addition to all three structures showing absorption maxima in the UV-Vis region.

Among the experimental studies already carried out, it is observed that the performance of perovskite halide double film devices is still inferior to Pb-based perovskite analogues. This fact may be associated with underdeveloped electronic structures, material properties, device architecture and quality of the films produced, since choosing a synthetic route to obtain uniform thin films with correct phase and composition is still a challenge.[138] Some examples with inorganic double perovskites in solar cell applications can be found in Table 3.

In addition to direct application in solar cells, these materials can also assume other related functions. The Cs_2PtI_6 structure, for example, has been investigated as a grain modifier in organic-inorganic hybrid PSC. Yang *et al*.[150] showed three main benefits of this action, these being: (*i*) increase in crystals with greater crystallinity by stimulating the growth of perovskite crystals;

Table 3. Double perovskites applied in solar cells

Perovskite	Synthesis method	Morphology	Film deposition method	Bandgap / eV	PCE / %	Reference
$Cs_2AgBiBr_6$	solution process	film	spin-coating	direct 2.21	2.43	43
$Cs_2AgBiBr_6$	solution process	film	vapor deposition	indirect 2.02	1.37	139
$Cs_2AgBiBr_6$	precipitation in solution - HBr	crystalline powder	low pressure assisted method	direct 2.05	1.44	140
$Cs_2AgBiBr_6$	precipitation in solution - HBr	crystalline powder	anti-solvent drip	direct –	2.23	132
$Cs_2AgBiBr_6$	precipitation in solution - HBr	crystalline powder	spin-coating	direct 2.20	1.26	134
$Cs_2AgBiBr_6$	modified solution process	crystalline powder	spin-coating	indirect 2.02	0.82	141
$Cs_2AgBiBr_6$	precipitation in solution - HBr	crystalline powder	solution processing	1.99	2.51	142
$Cs_2AgBiBr_6$	precipitation in solution - HBr	crystalline powder	vacuum sublimation	2.01	1.41	142
$Cs_2AgBiBr_6$	solution process	film	two-step heating process	2.02	2.84	136
$Cs_2AgBiBr_6$	hot-injection	nanocrystal	layer-by-layer deposition process	indirect 2.28	0.46	143
$Cs_2AgBiBr_6$:Sn	–	film	spin coating	–	2.74	144
$Cs_2AgBiBr_6$:H	solution process	film	spin coating	1.64	6.37	44
$Cs_2AgBi_{0.6}Sb_{0.4}Br_6$	hot-injection	nanocrystal	spin-coating	indirect 2.22 - DCB 2.26 - toluene	0.09	145
Cs_2NaBiI_6	hydrothermal (solvent processing)	crystalline powder	spin-coating	1.66	0.42	76
Cs_2TiBr_6	vapor-based method	film	vapor-based method	1.8	3.3	146
Cs_2SnI_6	modified solution process	crystalline powder	spin-coating	direct 1.48	0.86	147
$Cs_3Fe_2Cl_9$	solution process	nanocrystal	simple chemical process/ drop-casting	direct 2.73	0.6	148
$Cs_3Bi_2I_9$	solution process	nanocrystal	spin-coating	2.2	1.09	149

PCE: power conversion efficiency; DCB: 1,2-dichlorobenzene.

(*ii*) suppression of recombinations assisted by traps at grain boundaries due to heterojunction and interface passivation; and (*iii*) increased collection efficiency and mobility of carriers at grain boundaries, with carrier mobility found to be 2.83×10^3 cm^2 V^{-1} s^{-1}. Due to these benefits, it was possible to obtain a hybrid PSC with a PCE of 23.56%, of excellent thermoelectric quality and excellent stability even in high humidity, temperature and in acidic/basic media.

So far, very few fully inorganic double perovskites materials and no hybrid halides have been developed for optoelectronic applications, so there is a need to explore new stable B-site bimetallic double perovskites with narrower bandgap and ordered vacancy double perovskites for solar cell applications, aiming at a device architecture optimization. To achieve this, an improvement in the surface states of the crystals and active layers must also be sought.

5.2. Photocatalysis

$A_2B^IB^{III}X_6$ double perovskites have great potential in photocatalytic applications associated with their high stability (greater tolerance to humidity, temperature, and light), the long diffusion length of the carriers and the adequate position of the conduction band. Thus, the application of these in the photocatalytic reduction of CO_2, removal of NO, generation of H_2, degradation of dyes and acting as a photocatalyst in organic syntheses is investigated.[48,143]

The $Cs_2AgBiBr_6$ structure has been the most investigated to date. However, it has a large exciton binding energy, which is adverse for charge separation, limiting performance in photocatalytic reactions. The construction of heterostructures becomes an option to overcome this challenge.[151,152] Zhang *et al.*,[151] for example, inserted $Cs_2AgBiBr_6$ nanocrystals into MXene to perform CO_2 reduction. This improved light absorption due to the optical properties of the NCs and facilitated charge separation due to the electron transfer property of MXene. Furthermore, the heterostructure corroborates the suppression of electron-hole recombination.

Furthermore, before starting a photocatalytic reaction, the negative influence of organic ligands must be considered. These have advantages regarding the passivation of NCs' pendant bonds, which reduces surface defects. However, when at high density, these binders act as an insulating layer, thus blocking the mobility capacity of photogenerated charge and photoconversion products, which are easily accumulated in the binder shell. To achieve this, significant washing processes are important in order to reduce the density of surface binders.[18]

Another point to be evaluated is the morphology of the material, which can significantly affect its photocatalytic performance, changing the surface catalytic sites and charge mobility. Particularly, 2D structures, such as nanoplates, have unique physicochemical properties, such as phototransporters, anisotropic quantum confinement, defined surface atomic arrangements, which give them great photocatalytic potential. The significant performance of these structures is also related to the high percentage of surface atoms, with high mobility of free charge.[153] Table 4, below, presents some examples of work carried out in the area of photocatalysis.

In general, the activity of photocatalysts depends largely on their surface chemical states. Therefore, it is important that there be further investigations to optimize the chemical combination of the surface, as well as to better expose the most active sites on this surface.

Table 4. Double perovskites applied in photocatalysis

Perovskite	Synthesis method	Morphology	Bandgap / eV	Application	Total electron consumption	Reference
$Cs_2AgBiBr_6$	hot-injection	nanocrystal	indirect 2.52	CO_2 reduction	105 μmol g^{-1}	18
$Cs_2AgBiBr_6$	precursor injection at room temperature, followed by heating	nanoplates	indirect 2.06	CO_2 reduction	255.4 μmol g^{-1}	153
Cs_2AgBiI_6	antisolvent recrystallization	nanocrystal	indirect 1.82	CO_2 reduction	37.8 μmol g^{-1}	153
$Cs_2AgBiBr_6$-Cu-RGO	mechanochemically	nanoplates	indirect 2.0	CO_2 reduction	122 μmol g^{-1}	152
$Cs_2AgBiBr_6$-MXene	hot-injection	nanocrystal	–	CO_2 reduction	50.6 μmol g^{-1}	151
$Cs_2NaBiCl_6$	milling	microspheres	–	CO_2 reduction	–	154
$Cs_2AgBiBr_6$	hot-injection	nanocrystal	indirect 2.52	NO removal	–	155
$Cs_2AgBiBr_6$/RGO	aqueous solution	powder	–	H_2 generation	489 μmol g^{-1}	58
Cs_2SnI_6/Pt	one-pot hydrothermal	powder	1.22	H_2 generation	430 μmol g^{-1}	85
$Cs_2AgSbCl_6$	hot-injection	nanocrystal	2.63	organic synthesis catalysis	–	156
$Cs_2AgSbCl_6$	precipitation in solution - HCl	crystals	2.46	organic dye degradation	–	157
$Cs_2AgSbCl_6$	anti-solvent recrystallization	crystals	2.56	organic dye degradation	95.7%	157
$Cs_2AgBiBr_6$	precipitation in solution - HBr	powder	2.08	organic dye degradation	–	158
$Cs_2AgInCl_6$	precipitation in solution - HCl	crystals	3.33	degradation of organic pollutants	98.5%	159
Bi_2WO_6/$Cs_2AgBiBr_6$	hydrothermal, ball milling and thermal evaporation	nanocomposite	2.89/1.98	degradation of organic pollutants	97.4%	160

5.3. LED devices

When it comes to the applications of LED devices, it is important to highlight that for their high performance, materials with high PLQY are needed, which can be achieved by reducing the non-radiative recombination rate. This is the great challenge for the use of double perovskites, most of which have low natural photoluminescence. To overcome this problem, many researchers have used the doping and co-doping strategy. By adding impurities, the quantum confinement effect and defect modification can increase the rate of radiative recombinations, improving PLQY.[157]

Due to the properties of double perovskites, a more viable application would be in use as a phosphor for LEDs, for example, in downshifting in UV-LED chips, which function as a source of high-energy excitation light.[48] Antimony compounds, for example, can be applied as phosphor matrices due to their abundant resources, low price, stable chemical properties, excellent network rigidity and thermal stability. Thus, in recent studies of double perovskites applied in LEDs, this metal has been used as a doping agent.[157,161]

In addition to Sb^{3+} ions, the use of Eu^{3+} is recurrent in phosphors, in this case red color, due to the excellent color purity produced by their transitions. It should be noted that the luminescent performance of phosphorescent materials correlates with the movement of energy carriers and, therefore, an ideal matrix material is required to host the doping ions. In this case, $A_2B^IB^{III}X_6$ double perovskites are a suitable matrix, which can be structurally modulated, in addition to presenting relatively easy energy transfer when the B site is occupied by transition metals.[161] Bi^{3+} ions can also be used as luminescent doping materials, as was done in the Cs_2SnCl_6:Bi, structure, which can be applied as a blue emissive phosphor.[162] Table 5 presents some double perovskites applied in LED studies, and other examples can be seen in Table 2 presented in section 4.11.

Although there are already studies related to LED applications, many challenges still need to be resolved. Notable among them are the low PLQY of $A_2B^IB^{II}X_6$, crystals, long-term operating stability, lack of correlated color temperature (CCT) of high-quality warm white light below 4.000 K, and high enough color rendering index (CRI) (leading to search for red emission), required for indoor lighting.[48]

5.4. Other applications

Although studies aimed at the applications of double perovskites are still in their initial stages, there is already a diversification of areas in which these materials are being applied, as suggested in Table 6, due to their potential optoelectronic properties.

Among these properties, recently, Zhang and co-workers[169] revealed the occurrence of photochromism and afterglow in some double-doped perovskite single crystals. The existence of these phenomena can open a new window of applications for these materials, such as optical storage, security encryption and biological labeling.[170]

To expand the exploration of new potential applications of double perovskites, as well as for these applications to present satisfactory results, much work is still needed to understand the properties of these materials.

6. Future Challenges and Perspectives

Based on the contexts and references provided, it is evident that double perovskites offer promising perspectives. However, it is crucial to further discuss the main challenges for practical utilization of these materials. The quest for sustainable optoelectronic materials is essential, especially due to the instability and potential toxicity of lead-based perovskite. In this regard, double perovskites have emerged as potential substitutes.

Despite their notable characteristics (long charge

Table 5. Double perovskites applied in LED devices

Perovskite	Synthesis method	Morphology	Bandgap / eV	PLQY / %	Reference
Cs_2TiBr_6:Bi	hydrothermal/autoclave	powder	3.0	78.9	162
$Cs_2AgInCl_6$:Bi^{3+}	hot-injection	nanocrystal	4.71	31.4	163
$Cs_2AgInCl_6$:Bi^{3+}, Eu^{3+}	hot-injection	powder	3.1	80.1	164
$Cs2(Ag_{0.6}Na_{0.4})InCl_6$	hydrothermal/autoclave	powder	3.27	86	165
$Cs_2NaInCl_6$:Sb^{3+}	hot-injection	nano polycrystal	3.947	75	166
$Cs_2NaBiCl_6$: Eu^{3+}	hydrothermal	crystal	–	0.8	167
Ba_2CaWO_6:Mn^{4+}	solid state reaction	crystal	–	–	168
Cs_2NaYCl_6:Sb^{3+}, Eu^{3+}	hydrothermal/autoclave	single crystal	–	58.33	127

PLQY: photoluminescence quantum yield.

Table 6. Double perovskites applied in different areas

Perovskite	Synthesis method	Morphology	Bandgap	Application	Reference
$Cs_2AgInCl_6$	hydrothermal	single crystal	direct 3.2 eV	UV detectors	171
$Cs_2AgBiBr_6$	one-step spin-coating	thin film	–	photodetectors	172
$Cs_2AgInBr_6/SnO_2$	home-made low-pressure assisted method	film	–	stable UV and deep blue detector	173
Cs_2PdBr_6	precipitation with HBr	single crystal	1.6 eV	photodetectors	174
Cs_2SnI_6	hot-injection	nanocrystal	1.67 eV	photodetectors	175
Cs_2TeI_6	non-solution process	thin film	indirect 1.62 eV	gas sensor for NO_2	176
$Cs_2AgInBr_6$	inverse temperature crystallization	single crystal	indirect 2.1 eV	X-ray detectors	177
$Cs_2NaTbCl_6$	hydrothermal	crystals	–	X-ray detectors	178
Cs_2TeI_6	electrospray deposition	film	–	X-ray detectors	179
$Cs_2NaScCl_6$:Tb	hydrothermal	single crystal	–	radiation-storage battery	180

lifetime, adjustable bandgap, and viable syntheses under ambient conditions) halide double perovskites remain in the early research stages. Their modest publication output over the last five years, when compared to total perovskite studies, significantly affects device enhancement, and complicates equitable comparisons. Bearing this in perspective, it is essential to recognize that substitution may not be the forthcoming trend. The reason behind this is that lead perovskites have already established a significant presence in the field of optoelectronics, which has motivated scientists to concentrate on enhancing these devices. The pathway to widespread commercialization of simple perovskites is clearer than for their double counterparts, despite existing challenges. Consequently, it is likely that researchers will maintain a heightened interest in advancing single perovskite technologies, focusing on critical areas such as synthesis optimization to prevent secondary phases or polycrystalline films; enhancing resistance to external conditions like humidity, oxygen, heat, and light; and mitigating lead contamination.

It is also crucial to note that research at the frontier of scientific knowledge, such as double perovskite, carries inherent risks because of its unpredictable nature. While theoretical studies and calculations of structural stability provide some guidance, achieving practical success often remains limited. Furthermore, despite the new tolerance factor (τ) predicting thousands of double perovskites, the overwhelming majority of these are unlikely to exhibit the desired properties for successful optoelectronics applications.

As previously mentioned, the distance and symmetry of the MVB and MCB, along with parity-forbidden transitions, are one of materials limitations, resulting in predominantly weak electronic transitions. Regarding the bandgap limitations, this led to some publications characterized by a lack of clarity, insufficient research, or transparency concerning optoelectronic properties. Besides that, data often lack comparisons with other lead free or perovskite materials, making results appear more significant than they might be. However, since this paper did not aim to delve into these aspects, further directed review studies are necessary to systematize comparisons for each application.

As for vacancy perovskites, which undergo ligand-to-metal transitions and demonstrate stable iodides, they tend to exhibit a direct bandgap that is lower than those observed in conventional double perovskites. Nonetheless, a major limitation is the low metal density, which adversely affects device efficiency.

In the terms of the synthesis, the methods are well-known among researchers of single perovskites, including the possibility of employing simpler and less expensive techniques. This significantly enhances the prospects for in-depth research and high experiment repeatability. Moreover, it creates opportunities for groups with limited resources and for educational applications. On the other hand, for the improvement of properties, as shown, it may be necessary to use specific reagents and more sophisticated methods, which can significantly increase the cost of research.

Therefore, although researching double perovskites is extremely important, particularly for environmental considerations, it is essential to remain realistic about their prospects. Given their early stage of development, accurately predicting their true potential is challenging. Nevertheless, silver and bismuth bromides are the main

crystals studied and they are likely to be intensively investigated for future applications. Additionally, it is worth noting that luminous devices represent one of the most promising applications for double perovskites, particularly in the form of nanocrystal morphologies with the use of alloy and doping system combinations. Bearing this in mind, it is feasible that double perovskites could become commercially viable semiconductors in the future, yet whether they will replace lead halide perovskites remains uncertain. Determining their potential as substitutes is premature, and the crystals require further comprehensive research before application-focused investments can be initiated. In the upcoming years, investment in more established perovskites (e.g., lead iodides) will probably lead the market, with progress expected in the isolation and encapsulation methods for the metal core to reduce instability and toxicity.

7. Conclusions

The central aim of this review was to provide a clear and comprehensive source of content on double perovskites, from their history to prospects. Although these materials have recently gained prominence in scientific literature, they are not yet widely studied. There is a significant gap in research regarding their practical applications, and the true potential of most of these materials remains unknown, especially for crystals other than $Cs_2AgBiBr_6$. Beyond their initial state, one of the most significant contributions of double perovskites lies in the development of environmentally friendly materials. The key advantage is their versatility in combining elements and the ability to modulate properties through doping and alloying, owing to their resilience against impurities.

While it is premature to make definitive assertions, the role of double perovskites in optoelectronics could be significant in applications requiring long-term stability. This is particularly relevant in environments exposed to water and humidity, conditions under which traditional single perovskites exhibit greater instability. Applications such as hydrogen production and pollutant breakdown could benefit from the enhanced stability offered by double perovskites.

Nonetheless, the growing dependency on semiconductors in modern society suggests a broad spectrum of optoelectronic applications worth exploring, with sustainability and environmental safety being paramount. Therefore, studying double perovskites and related materials remains a vital area of research, offering considerable advances in optoelectronic applications and positive impacts on environmental and human health.

Acknowledgments

Financial support from FAPEMIG (Fundação de Amparo à Pesquisa do Estado de Minas Gerais), CNPq (Conselho Nacional de Desenvolvimento Científico e Tecnológico), and CAPES (Coordenação de Aperfeiçoamento de Pessoal de Nível Superior) are acknowledged.

***Igor Fernando L. Ferreira**, a graduate with a Bachelor's degree in Chemistry from the Federal University of São João del-Rei, is currently a Quality Manager at a tin smelting factory. As a member of the Material Chemistry Research Group (GPQM), he focused on lead-free semiconductors, particularly the synthesis and characterization of rudorfite (Ag_2BiI_5), and conducting a comprehensive literature review on double perovskites, under the guidance of Prof Dr Marco Antonio Schiavon.*

***Leticia F. Magalhães** is graduated in Chemistry Bachelor's degree from the Federal University of São João del-Rei (2016-2019). Master by the Graduate Program in Physics and Chemistry of Materials at the Federal University of São João Del-Rei (2020-2022), with the project: study of photophysical processes resulting from the interaction between $CsPbBr_3$ nanocrystals and the Rhodamine 6G dye. PhD student at the Graduate Program in Physics and Chemistry of Materials at the Federal University of São João Del-Rei (2022) and member of the Research Group in Materials Chemistry (GPQM) under the guidance of Prof Dr Marco Antonio Schiavon.*

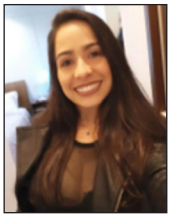

***Thaís Adriany S. Carvalho** is graduated in Chemical Engineering from the Federal University of São João Del-Rei (Brazil). Currently, she is a PhD student in Physics and Chemistry of Materials at the Federal University of São João Del-Rei and member of the Research Group in Materials Chemistry (GPQM). Her research interest focuses on synthesis and characterization of inorganic nanocrystals of lead-free perovskites, based on cesium and halides under the guidance of Prof Dr Marco Antonio Schiavon.*

***Marco Antonio Schiavon** is a chemist and obtained his PhD in 2002 at State University of Campinas (Brazil).*

Currently, he is a full professor of Inorganic Chemistry at Natural Sciences Department at the Federal University of São João del-Rei (Brazil). He is a research fellow of the National Council of Technological and Scientific Development-CNPq (Brazil). His research interest focuses on synthesis of semiconductor nanocrystals such as colloidal quantum dots and perovskite nanocrystals for energy conversion and understanding photoinduced processes employing optical spectroscopy techniques.

References

1. He, C.; Liu, X.; *Light: Sci. Appl.* **2023**, *12*, 15. [Crossref]
2. Ye, H.-Y.; Tang, Y.-Y.; Li, P.-F.; Liao, W.-Q.; Gao, J.-X.; Hua, X.-N.; Cai, H.; Shi, P.-P.; You, Y.-M.; Xiong, R.-G.; *Science* **2018**, *361*, 151. [Crossref]
3. Britvin, S. N.; Kashtanov, S. A.; Krzhizhanovskaya, M. G.; Gurinov, A. A.; Glumov, O. V.; Strekopytov, S.; Kretser, Y. L.; Zaitsev, A. N.; Chukanov, N. V.; Krivovichev, S. V.; *Angew. Chem., Int. Ed.* **2015**, *54*, 14340. [Crossref]
4. Lloyd II, A. J.; Hester, B. R.; Baxter, S. J.; Ma, S.; Prakapenka, V. B.; Tkachev, S. N.; Park, C.; Wilkinson, A. P.; *Chem. Mater.* **2021**, *33*, 3132. [Crossref]
5. Dong, H.; Ran, C.; Gao, W.; Li, M.; Xia, Y.; Huang, W.; *eLight* **2023**, *3*, 3. [Crossref]
6. Kojima, A.; Teshima, K.; Shirai, Y.; Miyasaka, T.; *J. Am. Chem. Soc.* **2009**, *131*, 6050. [Crossref]
7. Jeong, J.; Kim, M.; Seo, J.; Lu, H.; Ahlawat, P.; Mishra, A.; Yang, Y.; Hope, M. A.; Eickemeyer, F. T.; Kim, M.; Yoon, Y. J.; Choi, I. W.; Darwich, B. P.; Choi, S. J.; Jo, Y.; Lee, J. H.; Walker, B.; Zakeeruddin, S. M.; Emsley, L.; Rothlisberger, U.; Hagfeldt, A.; Kim, D. S.; Grätzel, M.; Kim, J. Y.; *Nature* **2021**, *592*, 381. [Crossref]
8. NREL, *Best Research-Cell Efficiency Chart*, https://www.nrel.gov/pv/cell-efficiency.html, accessed in May 2024.
9. Huang, H.; Pradhan, B.; Hofkens, J.; Roeffaers, M. B. J.; Steele, J. A.; *ACS Energy Lett.* **2020**, *5*, 1107. [Crossref]
10. Dong, H.; Zhang, C.; Liu, X.; Yao, J.; Zhao, Y. S.; *Chem. Soc. Rev.* **2020**, *49*, 951. [Crossref]
11. Huynh, K. A.; Nguyen, D. L. T.; Nguyen, V.; Vo, D. N.; Trinh, Q. T.; Nguyen, T. P.; Kim, S. Y.; Le, Q. V.; *J. Chem. Technol. Biotechnol.* **2020**, *95*, 2579. [Crossref]
12. Kar, S.; Jamaludin, N. F.; Yantara, N.; Mhaisalkar, S. G.; Leong, W. L.; *Nanophotonics* **2021**, *10*, 2103. [Crossref]
13. Akkerman, Q. A.; Manna, L.; *ACS Energy Lett.* **2020**, *5*, 604. [Crossref]
14. Ghosh, S.; Shankar, H.; Kar, P.; *Mater. Adv.* **2022**, *3*, 3742. [Crossref]
15. Ponti, C.; Nasti, G.; Di Girolamo, D.; Cantone, I.; Alharthi, F. A.; Abate, A.; *Trends Ecol. Evol.* **2022**, *37*, 281. [Crossref]
16. Lidsky, T. I.; Schneider, J. S.; *Brain* **2003**, *126*, 5. [Crossref]
17. Ren, M.; Qian, X.; Chen, Y.; Wang, T.; Zhao, Y.; *J. Hazard. Mater.* **2022**, *426*, 127848. [Crossref]
18. Zhou, L.; Xu, Y.-F.; Chen, B.-X.; Kuang, D.-B.; Su, C.-Y.; *Small* **2018**, *14*, 1703762. [Crossref]
19. Aldamasy, M.; Iqbal, Z.; Li, G.; Pascual, J.; Alharthi, F.; Abate, A.; Li, M.; *Phys. Chem. Chem. Phys.* **2021**, *23*, 23413. [Crossref]
20. Nishimura, K.; Kamarudin, M. A.; Hirotani, D.; Hamada, K.; Shen, Q.; Iikubo, S.; Minemoto, T.; Yoshino, K.; Hayase, S.; *Nano Energy* **2020**, *74*, 104858. [Crossref]
21. Hoye, R. L. Z.; Hidalgo, J.; Jagt, R. A.; Correa-Baena, J.; Fix, T.; MacManus-Driscoll, J. L.; *Adv. Energy Mater.* **2022**, *12*, 2100499. [Crossref]
22. Wolf, N. R.; Connor, B. A.; Slavney, A. H.; Karunadasa, H. I.; *Angew. Chem.* **2021**, *133*, 16400. [Crossref]
23. Ji, F.; Boschloo, G.; Wang, F.; Gao, F.; *Solar RRL* **2023**, *7*, 2201112. [Crossref]
24. Chakhmouradian, A. R.; Woodward, P. M.; *Phys. Chem. Minerals* **2014**, *41*, 387. [Crossref]
25. Goldschmidt, V. M.; *Naturwissenschaften* **1926**, *14*, 477. [Crossref]
26. Haertling, G. H.; *J. Am. Ceram. Soc.* **1999**, *82*, 797. [Crossref]
27. Callister, W. D.; Rethwisch, D. G.; *Materials Science and Engineering: An Introduction*, 9th ed.; Wiley: Hoboken, NJ, 2014.
28. Møller, C. K.; *Nature* **1958**, *182*, 1436. [Crossref]
29. Protesescu, L.; Yakunin, S.; Bodnarchuk, M. I.; Krieg, F.; Caputo, R.; Hendon, C. H.; Yang, R. X.; Walsh, A.; Kovalenko, M. V.; *Nano Lett.* **2015**, *15*, 3692. [Crossref]
30. Ghasemi, M.; Hao, M.; Xiao, M.; Chen, P.; He, D.; Zhang, Y.; Chen, W.; Fan, J.; Yun, J. H.; Jia, B.; Wen, X.; *Nanophotonics* **2021**, *10*, 2181. [Crossref]
31. Nechache, R.; Harnagea, C.; Li, S.; Cardenas, L.; Huang, W.; Chakrabartty, J.; Rosei, F.; *Nature Photon.* **2015**, *9*, 61. [Crossref]
32. Wells, H. L.; *Am. J. Sci.* **1922**, *s5-3*, 315. [Link] accessed in May 2024
33. Elliott, N.; Pauling, L.; *J. Am. Chem. Soc.* **1938**, *60*, 1846. [Crossref]
34. Berzelius, J. J.; *Ann. Phys. Chem.* **1834**, *108*, 577. [Crossref]
35. Lee, B.; Stoumpos, C. C.; Zhou, N.; Hao, F.; Malliakas, C.; Yeh, C.-Y.; Marks, T. J.; Kanatzidis, M. G.; Chang, R. P. H.; *J. Am. Chem. Soc.* **2014**, *136*, 15379. [Crossref]
36. Qiu, X.; Cao, B.; Yuan, S.; Chen, X.; Qiu, Z.; Jiang, Y.; Ye, Q.; Wang, H.; Zeng, H.; Liu, J.; Kanatzidis, M. G.; *Sol. Energy Mater. Sol. Cells* **2017**, *159*, 227. [Crossref]
37. Volonakis, G.; Filip, M. R.; Haghighirad, A. A.; Sakai, N.; Wenger, B.; Snaith, H. J.; Giustino, F.; *J. Phys. Chem. Lett.* **2016**, *7*, 1254. [Crossref]

38. McClure, E. T.; Ball, M. R.; Windl, W.; Woodward, P. M.; *Chem. Mater.* **2016**, *28*, 1348. [Crossref]
39. Slavney, A. H.; Hu, T.; Lindenberg, A. M.; Karunadasa, H. I.; *J. Am. Chem. Soc.* **2016**, *138*, 2138. [Crossref]
40. Slavney, A. H.; Leppert, L.; Saldivar Valdes, A.; Bartesaghi, D.; Savenije, T. J.; Neaton, J. B.; Karunadasa, H. I.; *Angew. Chem., Int. Ed.* **2018**, *57*, 12765. [Crossref]
41. Connor, B. A.; Leppert, L.; Smith, M. D.; Neaton, J. B.; Karunadasa, H. I.; *J. Am. Chem. Soc.* **2018**, *140*, 5235. [Crossref]
42. Slavney, A. H.; Connor, B. A.; Leppert, L.; Karunadasa, H. I.; *Chem. Sci.* **2019**, *10*, 11041. [Crossref]
43. Greul, E.; Petrus, M. L.; Binek, A.; Docampo, P.; Bein, T.; *J. Mater. Chem. A* **2017**, *5*, 19972. [Crossref]
44. Zhang, Z.; Sun, Q.; Lu, Y.; Lu, F.; Mu, X.; Wei, S.-H.; Sui, M.; *Nat. Commun.* **2022**, *13*, 3397. [Crossref]
45. Rühle, S.; *Solar Energy* **2016**, *130*, 139. [Crossref]
46. Alanazi, T. I.; *Crystals* **2023**, *13*, 267. [Crossref]
47. Creutz, S. E.; Crites, E. N.; De Siena, M. C.; Gamelin, D. R.; *Nano Lett.* **2018**, *18*, 1118. [Crossref]
48. Wu, S.; Liu, Y.; *Nano Res.* **2023**, *16*, 5572. [Crossref]
49. de Souza Carvalho, T. A.; Magalhaes, L. F.; Santos, C. I. L.; de Freitas, T. A. Z.; Carvalho Vale, B. R.; Vale da Fonseca, A. F.; Schiavon, M. A.; *Chem. – Eur. J.* **2023**, *29*, e202202518. [Crossref]
50. Bai, T.; Wang, X.; Wang, Z.; Ji, S.; Meng, X.; Wang, Q.; Zhang, R.; Han, P.; Han, K.; Chen, J.; Liu, F.; Yang, B.; *Angew. Chem., Int. Ed.* **2023**, *62*, e202213240. [Crossref]
51. Dai, Q.; Duty, C. E.; Hu, M. Z.; *Small* **2010**, *6*, 1577. [Crossref]
52. Luo, J.; Wang, X.; Li, S.; Liu, J.; Guo, Y.; Niu, G.; Yao, L.; Fu, Y.; Gao, L.; Dong, Q.; Zhao, C.; Leng, M.; Ma, F.; Liang, W.; Wang, L.; Jin, S.; Han, J.; Zhang, L.; Etheridge, J.; Wang, J.; Yan, Y.; Sargent, E. H.; Tang, J.; *Nature* **2018**, *563*, 541. [Crossref]
53. Li, X.; Wang, D.; Zhong, Y.; Jiang, F.; Zhao, D.; Sun, S.; Lu, P.; Lu, M.; Wang, Z.; Wu, Z.; Gao, Y.; Zhang, Y.; Yu, W. W.; Bai, X.; *Adv. Sci.* **2023**, *10*, 2207571. [Crossref]
54. Zhang, Y.; Sun, Z.; Wang, Z.; Zang, Y.; Tao, X.; *Int. J. Hydrogen Energy* **2022**, *47*, 8829. [Crossref]
55. Wu, D.; Zhao, X.; Huang, Y.; Lai, J.; Li, H.; Yang, J.; Tian, C.; He, P.; Huang, Q.; Tang, X.; *Chem. Mater.* **2021**, *33*, 4971. [Crossref]
56. Li, X.; Mai, H.; Cox, N.; Lu, J.; Wen, X.; Chen, D.; Caruso, R. A.; *Chem. Mater.* **2023**, *35*, 3105. [Crossref]
57. Jiang, Y.; Li, K.; Wu, X.; Zhu, M.; Zhang, H.; Zhang, K.; Wang, Y.; Loh, K. P.; Shi, Y.; Xu, Q.-H.; *ACS Appl. Mater. Interfaces* **2021**, *13*, 10037. [Crossref]
58. Wang, T.; Yue, D.; Li, X.; Zhao, Y.; *Appl. Catal., B* **2020**, *268*, 118399. [Crossref]
59. Raphael, E.; Silva, M. N.; Szostak, R.; Schiavon, M. A.; Nogueira, A. F.; *Quim. Nova* **2018**, *41*, 61. [Crossref]
60. Pandey, N.; Neelu, N.; Chakrabarti, S.; *Opt. Mater.* **2023**, *137*, 113570. [Crossref]
61. Maughan, A. E.; Ganose, A. M.; Scanlon, D. O.; Neilson, J. R.; *Chem. Mater.* **2019**, *31*, 1184. [Crossref]
62. Prassides, K.; Day, P.; Cheetham, A. K.; *Inorg. Chem.* **1985**, *24*, 545. [Crossref]
63. Atkinson, L.; Day, P.; *J. Chem. Soc., A* **1969**, 2423. [Crossref]
64. King, G.; Woodward, P. M.; *J. Mater. Chem.* **2010**, *20*, 5785. [Crossref]
65. Anderson, M.; Greenwood, K.; Taylor, G.; Poeppelmeier, K.; *Prog. Solid State Chem.* **1993**, *22*, 197. [Crossref]
66. Ji, G.; Han, C.; Hu, S.; Fu, P.; Chen, X.; Guo, J.; Tang, J.; Xiao, Z.; *J. Am. Chem. Soc.* **2021**, *143*, 10275. [Crossref]
67. Yang, J.; Zhang, P.; Wei, S.-H.; *J. Phys. Chem. Lett.* **2018**, *9*, 31. [Crossref]
68. Muscarella, L. A.; Hutter, E. M.; *ACS Energy Lett.* **2022**, *7*, 2128. [Crossref]
69. Vishnoi, P.; Seshadri, R.; Cheetham, A. K.; *J. Phys. Chem. C* **2021**, *125*, 11756. [Crossref]
70. Mao, L.; Teicher, S. M. L.; Stoumpos, C. C.; Kennard, R. M.; DeCrescent, R. A.; Wu, G.; Schuller, J. A.; Chabinyc, M. L.; Cheetham, A. K.; Seshadri, R.; *J. Am. Chem. Soc.* **2019**, *141*, 19099. [Crossref]
71. Vishnoi, P.; Zuo, J. L.; Li, X.; Binwal, D. C.; Wyckoff, K. E.; Mao, L.; Kautzsch, L.; Wu, G.; Wilson, S. D.; Kanatzidis, M. G.; Seshadri, R.; Cheetham, A. K.; *J. Am. Chem. Soc.* **2022**, *144*, 6661. [Crossref]
72. Deng, Z.; Wei, F.; Sun, S.; Kieslich, G.; Cheetham, A. K.; Bristowe, P. D.; *J. Mater. Chem. A* **2016**, *4*, 12025. [Crossref]
73. Su, C.-Y.; Yao, Y.-F.; Zhang, Z.-X.; Wang, Y.; Chen, M.; Huang, P.-Z.; Zhang, Y.; Qiao, W.-C.; Fu, D.-W.; *Chem. Sci.* **2022**, *13*, 4794. [Crossref]
74. Jana, M. K.; Janke, S. M.; Dirkes, D. J.; Dovletgeldi, S.; Liu, C.; Qin, X.; Gundogdu, K.; You, W.; Blum, V.; Mitzi, D. B.; *J. Am. Chem. Soc.* **2019**, *141*, 7955. [Crossref]
75. Cheng, P.; Wu, T.; Li, Y.; Jiang, L.; Deng, W.; Han, K.; *New J. Chem.* **2017**, *41*, 9598. [Crossref]
76. Zhang, C.; Gao, L.; Teo, S.; Guo, Z.; Xu, Z.; Zhao, S.; Ma, T.; *Sustainable Energy Fuels* **2018**, *2*, 2419. [Crossref]
77. Gou, G.; Charles, N.; Shi, J.; Rondinelli, J. M.; *Inorg. Chem.* **2017**, *56*, 11854. [Crossref]
78. Aimi, A.; Mori, D.; Hiraki, K.; Takahashi, T.; Shan, Y. J.; Shirako, Y.; Zhou, J.; Inaguma, Y.; *Chem. Mater.* **2014**, *26*, 2601. [Crossref]
79. Subramanian, M. A.; Li, D.; Duan, N.; Reisner, B. A.; Sleight, A. W.; *J. Solid State Chem.* **2000**, *151*, 323. [Crossref]
80. Inaguma, Y.; Liquan, C.; Itoh, M.; Nakamura, T.; Uchida, T.; Ikuta, H.; Wakihara, M.; *Solid State Commun.* **1993**, *86*, 689. [Crossref]
81. Yamada, I.; Tsuchida, K.; Ohgushi, K.; Hayashi, N.; Kim, J.; Tsuji, N.; Takahashi, R.; Matsushita, M.; Nishiyama, N.; Inoue, T.; Irifune, T.; Kato, K.; Takata, M.; Takano, M.; *Angew. Chem., Int. Ed.* **2011**, *50*, 6579. [Crossref]

82. Rahim, W.; Cheng, A.; Lyu, C.; Shi, T.; Wang, Z.; Scanlon, D. O.; Palgrave, R. G.; *Chem. Mater.* **2020**, *32*, 9573. [Crossref]
83. Jodlowski, AlexanderD.; Rodríguez-Padrón, D.; Luque, R.; De Miguel, G.; *Adv. Energy Mater.* **2018**, *8*, 1703120. [Crossref]
84. Ma, X.; Li, Z.; *Phys. Status Solidi* **2019**, *256*, 1800427. [Crossref]
85. Zhou, P.; Chen, H.; Chao, Y.; Zhang, Q.; Zhang, W.; Lv, F.; Gu, L.; Zhao, Q.; Wang, N.; Wang, J.; Guo, S.; *Nat. Commun.* **2021**, *12*, 4412. [Crossref]
86. Zhao, Y.; Cruse, K.; Abdelsamie, M.; Ceder, G.; Sutter-Fella, C. M.; *Matter* **2021**, *4*, 1801. [Crossref]
87. Lei, H.; Hardy, D.; Gao, F.; *Adv. Funct. Mater.* **2021**, *31*, 2105898. [Crossref]
88. Bekenstein, Y.; Dahl, J. C.; Huang, J.; Osowiecki, W. T.; Swabeck, J. K.; Chan, E. M.; Yang, P.; Alivisatos, A. P.; *Nano Lett.* **2018**, *18*, 3502. [Crossref]
89. Locardi, F.; Cirignano, M.; Baranov, D.; Dang, Z.; Prato, M.; Drago, F.; Ferretti, M.; Pinchetti, V.; Fanciulli, M.; Brovelli, S.; De Trizio, L.; Manna, L.; *J. Am. Chem. Soc.* **2018**, *140*, 12989. [Crossref]
90. Wang, C.; Liu, Y.; Guo, Y.; Ma, L.; Liu, Y.; Zhou, C.; Yu, X.; Zhao, G.; *Chem. Eng. J.* **2020**, *397*, 125367. [Crossref]
91. Singh, S.; Khan, Z. H.; Khan, M. B.; Kumar, P.; Kumar, P.; *Bull. Mater. Sci.* **2022**, *45*, 81. [Crossref]
92. Liu, Y.; Jing, Y.; Zhao, J.; Liu, Q.; Xia, Z.; *Chem. Mater.* **2019**, *31*, 3333. [Crossref]
93. Zhang, B.; Wang, M.; Ghini, M.; Melcherts, A. E. M.; Zito, J.; Goldoni, L.; Infante, I.; Guizzardi, M.; Scotognella, F.; Kriegel, I.; De Trizio, L.; Manna, L.; *ACS Materials Lett.* **2020**, *2*, 1442. [Crossref]
94. De Roo, J.; Ibáñez, M.; Geiregat, P.; Nedelcu, G.; Walravens, W.; Maes, J.; Martins, J. C.; Van Driessche, I.; Kovalenko, M. V.; Hens, Z.; *ACS Nano* **2016**, *10*, 2071. [Crossref]
95. Zhang, Y.; Shah, T.; Deepak, F. L.; Korgel, B. A.; *Chem. Mater.* **2019**, *31*, 7962. [Crossref]
96. Dahl, J. C.; Osowiecki, W. T.; Cai, Y.; Swabeck, J. K.; Bekenstein, Y.; Asta, M.; Chan, E. M.; Alivisatos, A. P.; *Chem. Mater.* **2019**, *31*, 3134. [Crossref]
97. Zheng, K.; Chen, B.; Xie, L.; Li, X.; Lu, B.; Wang, M.; Wu, Y.; Jiang, T.; Zhang, F.; Li, X.; Wang, Y.; *Adv. Optical Mater.* **2022**, *10*, 2101661. [Crossref]
98. Kim, K.; Kim, H.; Park, J.; *ACS Omega* **2021**, *6*, 26952. [Crossref]
99. Usman, M.; Yan, Q.; *Crystals* **2020**, *10*, 62. [Crossref]
100. Li, C.; Lu, X.; Ding, W.; Feng, L.; Gao, Y.; Guo, Z.; *Acta Crystallogr., Sect. B: Struct. Sci.* **2008**, *64*, 702. [Crossref]
101. Zhao, X.-G.; Yang, D.; Sun, Y.; Li, T.; Zhang, L.; Yu, L.; Zunger, A.; *J. Am. Chem. Soc.* **2017**, *139*, 6718. [Crossref]
102. Wu, Y.; Li, X.; Zeng, H.; *Small Struct.* **2021**, *2*, 2000071. [Crossref]
103. Lee, J.-H.; Bristowe, N. C.; Lee, J. H.; Lee, S.-H.; Bristowe, P. D.; Cheetham, A. K.; Jang, H. M.; *Chem. Mater.* **2016**, *28*, 4259. [Crossref]
104. Bartel, C. J.; Sutton, C.; Goldsmith, B. R.; Ouyang, R.; Musgrave, C. B.; Ghiringhelli, L. M.; Scheffler, M.; *Sci. Adv.* **2019**, *5*, eaav0693. [Crossref]
105. Boysen, H.; Hewat, A. W.; *Acta Crystallogr., Sect. B: Struct. Sci.* **1978**, *34*, 1412. [Crossref]
106. Fedorovskiy, A. E.; Drigo, N. A.; Nazeeruddin, M. K.; *Small Methods* **2020**, *4*, 1900426. [Crossref]
107. Xiao, Z.; Meng, W.; Wang, J.; Mitzi, D. B.; Yan, Y.; *Mater. Horiz.* **2017**, *4*, 206. [Crossref]
108. Yang, B.; Mao, X.; Hong, F.; Meng, W.; Tang, Y.; Xia, X.; Yang, S.; Deng, W.; Han, K.; *J. Am. Chem. Soc.* **2018**, *140*, 17001. [Crossref]
109. Yang, B.; Chen, J.; Yang, S.; Hong, F.; Sun, L.; Han, P.; Pullerits, T.; Deng, W.; Han, K.; *Angew. Chem., Int. Ed.* **2018**, *57*, 5359. [Crossref]
110. Zhou, J.; Rong, X.; Zhang, P.; Molokeev, M. S.; Wei, P.; Liu, Q.; Zhang, X.; Xia, Z.; *Adv. Optical Mater.* **2019**, *7*, 1801435. [Crossref]
111. Xiao, Z.; Song, Z.; Yan, Y.; *Adv. Mater.* **2019**, *31*, 1803792. [Crossref]
112. Zhao, X.-G.; Yang, J.-H.; Fu, Y.; Yang, D.; Xu, Q.; Yu, L.; Wei, S.-H.; Zhang, L.; *J. Am. Chem. Soc.* **2017**, *139*, 2630. [Crossref]
113. Delor, M.; Slavney, A. H.; Wolf, N. R.; Filip, M. R.; Neaton, J. B.; Karunadasa, H. I.; Ginsberg, N. S.; *ACS Energy Lett.* **2020**, *5*, 1337. [Crossref]
114. Volonakis, G.; Haghighirad, A. A.; Snaith, H. J.; Giustino, F.; *J. Phys. Chem. Lett.* **2017**, *8*, 3917. [Crossref]
115. Ji, F.; Klarbring, J.; Wang, F.; Ning, W.; Wang, L.; Yin, C.; Figueroa, J. S. M.; Christensen, C. K.; Etter, M.; Ederth, T.; Sun, L.; Simak, S. I.; Abrikosov, I. A.; Gao, F.; *Angew. Chem., Int. Ed.* **2020**, *59*, 15191. [Crossref]
116. Bartie, N. J.; Cobos-Becerra, Y. L.; Fröhling, M.; Schlatmann, R.; Reuter, M. A.; *Resour., Conserv. Recycl.* **2021**, *169*, 105516. [Crossref]
117. Hoye, R. L. Z.; Eyre, L.; Wei, F.; Brivio, F.; Sadhanala, A.; Sun, S.; Li, W.; Zhang, K. H. L.; MacManus-Driscoll, J. L.; Bristowe, P. D.; Friend, R. H.; Cheetham, A. K.; Deschler, F.; *Adv. Materials Inter.* **2018**, *5*, 1800464. [Crossref]
118. Meng, W.; Wang, X.; Xiao, Z.; Wang, J.; Mitzi, D. B.; Yan, Y.; *J. Phys. Chem. Lett.* **2017**, *8*, 2999. [Crossref]
119. Weller, M.; Overton, T.; Rourke, J.; Armstrong, F. A.; *Inorganic Chemistry*, 6th ed.; Oxford University Press: Oxford, 2014.
120. Cao, L.; Jia, X.; Gan, W.; Ma, C.; Zhang, J.; Lou, B.; Wang, J.; *Adv. Funct. Materials* **2023**, *33*, 2212135. [Crossref]
121. Du, K.; Meng, W.; Wang, X.; Yan, Y.; Mitzi, D. B.; *Angew. Chem., Int. Ed.* **2017**, *56*, 8158. [Crossref]
122. Wan, H.; Jia, F.; Dinic, F.; Imran, M.; Rehl, B.; Liu, Y.;

Paritmongkol, W.; Xia, P.; Wang, Y.-K.; Liu, Y.; Wang, S.; Lyu, Q.; Cotella, G. F.; Chun, P.; Voznyy, O.; Hoogland, S.; Sargent, E. H.; *Chem. Mater.* **2023**, *35*, 948. [Crossref]

123. Ji, F.; Huang, Y.; Wang, F.; Kobera, L.; Xie, F.; Klarbring, J.; Abbrent, S.; Brus, J.; Yin, C.; Simak, S. I.; Abrikosov, I. A.; Buyanova, I. A.; Chen, W. M.; Gao, F.; *Adv. Funct. Mater.* **2020**, *30*, 2005521. [Crossref]
124. Li, L.; Shao, H.; Wu, X.; Chen, W.; Zhu, J.; Dong, B.; Xu, L.; Xu, W.; Hu, J.; Zhou, M.; Ji, Y.; Song, H.; Bai, X.; *Mater. Res. Bull.* **2022**, *147*, 111645. [Crossref]
125. Liao, Q.; Chen, J.; Zhou, L.; Wei, T.; Zhang, L.; Chen, D.; Huang, F.; Pang, Q.; Zhang, J. Z.; *J. Phys. Chem. Lett.* **2020**, *11*, 8392. [Crossref]
126. Ji, F.; Wang, F.; Kobera, L.; Abbrent, S.; Brus, J.; Ning, W.; Gao, F.; *Chem. Sci.* **2021**, *12*, 1730. [Crossref]
127. Wang, Y.; Bai, S.; Liang, H.; Li, C.; Tan, T.; Yang, G.; Wang, J.; *J. Alloys Compd.* **2023**, *934*, 167952. [Crossref]
128. Ganose, A.; *Atomic-Scale Insights into Emergent Photovoltaic Absorbers*; Springer International Publishing: Cham, 2020.
129. Zhao, X.; Liu, T.; Loo, Y.; *Adv. Mater.* **2022**, *34*, 2105849. [Crossref]
130. Zhao, X.; Liu, T.; Kaplan, A. B.; Yao, C.; Loo, Y.-L.; *Nano Lett.* **2020**, *20*, 8880. [Crossref]
131. Sirtl, M. T.; Hooijer, R.; Armer, M.; Ebadi, F. G.; Mohammadi, M.; Maheu, C.; Weis, A.; Van Gorkom, B. T.; Häringer, S.; Janssen, R. A. J.; Mayer, T.; Dyakonov, V.; Tress, W.; Bein, T.; *Adv. Energy Mater.* **2022**, *12*, 2103215. [Crossref]
132. Gao, W.; Ran, C.; Xi, J.; Jiao, B.; Zhang, W.; Wu, M.; Hou, X.; Wu, Z.; *ChemPhysChem* **2018**, *19*, 1696. [Crossref]
133. Mahmood, Q.; Hassan, M.; Flemban, T. H.; Ul Haq, B.; AlFaify, S.; Kattan, N. A.; Laref, A.; *J. Phys. Chem. Solids* **2021**, *148*, 109665. [Crossref]
134. Pantaler, M.; Cho, K. T.; Queloz, V. I. E.; García Benito, I.; Fettkenhauer, C.; Anusca, I.; Nazeeruddin, M. K.; Lupascu, D. C.; Grancini, G.; *ACS Energy Lett.* **2018**, *3*, 1781. [Crossref]
135. Wang, B.; Li, N.; Yang, L.; Dall'Agnese, C.; Jena, A. K.; Miyasaka, T.; Wang, X.-F.; *J. Am. Chem. Soc.* **2021**, *143*, 14877. [Crossref]
136. Yang, X.; Chen, Y.; Liu, P.; Xiang, H.; Wang, W.; Ran, R.; Zhou, W.; Shao, Z.; *Adv. Funct. Mater.* **2020**, *30*, 2001557. [Crossref]
137. Hakami, O.; *Int. J. Energy Res.* **2022**, *46*, 11326. [Crossref]
138. Chu, L.; Ahmad, W.; Liu, W.; Yang, J.; Zhang, R.; Sun, Y.; Yang, J.; Li, X.; *Nano-Micro Lett.* **2019**, *11*, 16. [Crossref]
139. Wang, M.; Zeng, P.; Bai, S.; Gu, J.; Li, F.; Yang, Z.; Liu, M.; *Solar RRL* **2018**, *2*, 1800217. [Crossref]
140. Wu, C.; Zhang, Q.; Liu, Y.; Luo, W.; Guo, X.; Huang, Z.; Ting, H.; Sun, W.; Zhong, X.; Wei, S.; Wang, S.; Chen, Z.; Xiao, L.; *Adv. Sci.* **2018**, *5*, 1700759. [Crossref]
141. Kentsch, R.; Scholz, M.; Horn, J.; Schlettwein, D.; Oum, K.; Lenzer, T.; *J. Phys. Chem. C* **2018**, *122*, 25940. [Crossref]
142. Igbari, F.; Wang, R.; Wang, Z.-K.; Ma, X.-J.; Wang, Q.; Wang, K.-L.; Zhang, Y.; Liao, L.-S.; Yang, Y.; *Nano Lett.* **2019**, *19*, 2066. [Crossref]
143. Ahmad, R.; Nutan, G. V.; Singh, D.; Gupta, G.; Soni, U.; Sapra, S.; Srivastava, R.; *Nano Res.* **2021**, *14*, 1126. [Crossref]
144. Dehingia, A.; Das, U.; Roy, A.; *J. Mater. Chem. C* **2023**, *11*, 15347. [Crossref]
145. Kumar, A.; Swami, S. K.; Rawat, S. S.; Singh, V. N.; Sinha, O. P.; Srivastava, R.; *Int. J. Energy Res.* **2021**, *45*, 16769. [Crossref]
146. Chen, M.; Ju, M.-G.; Carl, A. D.; Zong, Y.; Grimm, R. L.; Gu, J.; Zeng, X. C.; Zhou, Y.; Padture, N. P.; *Joule* **2018**, *2*, 558. [Crossref]
147. Qiu, X.; Jiang, Y.; Zhang, H.; Qiu, Z.; Yuan, S.; Wang, P.; Cao, B.; *Phys. Status Solidi RRL* **2016**, *10*, 587. [Crossref]
148. Jassim, S. M.; *J. Electron. Mater.* **2022**, *51*, 2828. [Crossref]
149. Park, B.; Philippe, B.; Zhang, X.; Rensmo, H.; Boschloo, G.; Johansson, E. M. J.; *Adv. Mater.* **2015**, *27*, 6806. [Crossref]
150. Yang, S.; Han, Q.; Wang, L.; Zhou, Y.; Yu, F.; Li, C.; Cai, X.; Gao, L.; Zhang, C.; Ma, T.; *Chem. Eng. J.* **2021**, *426*, 131838. [Crossref]
151. Zhang, Z.; Wang, B.; Zhao, H.-B.; Liao, J.-F.; Zhou, Z.-C.; Liu, T.; He, B.; Wei, Q.; Chen, S.; Chen, H.-Y.; Kuang, D.-B.; Li, Y.; Xing, G.; *Appl. Catal., B* **2022**, *312*, 121358. [Crossref]
152. Kumar, S.; Hassan, I.; Regue, M.; Gonzalez-Carrero, S.; Rattner, E.; Isaacs, M. A.; Eslava, S.; *J. Mater. Chem. A* **2021**, *9*, 12179. [Crossef]
153. Liu, Z.; Yang, H.; Wang, J.; Yuan, Y.; Hills-Kimball, K.; Cai, T.; Wang, P.; Tang, A.; Chen, O.; *Nano Lett.* **2021**, *21*, 1620. [Crossref]
154. Pi, J.; Jia, X.; Long, Z.; Yang, S.; Wu, H.; Zhou, D.; Wang, Q.; Zheng, H.; Yang, Y.; Zhang, J.; Qiu, J.; *Adv. Energy Mater.* **2022**, *12*, 2270179. [Crossref]
155. Wu, D.; Tao, Y.; Huang, Y.; Huo, B.; Zhao, X.; Yang, J.; Jiang, X.; Huang, Q.; Dong, F.; Tang, X.; *J. Catal.* **2021**, *397*, 27. [Crossref]
156. Guo, Y.; Lou, Y.; Chen, J.; Zhao, Y.; *ChemSusChem* **2022**, *15*, e202102334. [Crossref]
157. Guo, K.; Lin, P.; Wu, D.; Shi, Z.; Chen, X.; Han, Y.; Tian, Y.; Li, X.; *Chem.- Eur. J.* **2023**, *29*, e202300400. [Crossref]
158. Zhang, Z.; Liang, Y.; Huang, H.; Liu, X.; Li, Q.; Chen, L.; Xu, D.; *Angew. Chem., Int. Ed.* **2019**, *58*, 7263. [Crossref]
159. Li, K.; Li, S.; Zhang, W.; Shi, Z.; Wu, D.; Chen, X.; Lin, P.; Tian, Y.; Li, X.; *J. Colloid Interface Sci.* **2021**, *596*, 376. [Crossref]
160. Zhang, H.; Ji, X.; Xu, H.; Zhang, R.; Li, Y.; Chen, Q.; *J. Alloys Compd.* **2023**, *968*, 172132. [Crossref]
161. Geng, X.; Xie, Y.; Ma, Y.; Liu, Y.; Luo, J.; Wang, J.; Yu, R.; Deng, B.; Zhou, W.; *J. Alloys Compd.* **2020**, *847*, 156249. [Crossref]
162. Tan, Z.; Li, J.; Zhang, C.; Li, Z.; Hu, Q.; Xiao, Z.; Kamiya, T.; Hosono, H.; Niu, G.; Lifshitz, E.; Cheng, Y.; Tang, J.; *Adv. Funct. Mater.* **2018**, *28*, 1801131. [Crossref]

163. Zhang, Y.; Zhang, Z.; Yu, W.; He, Y.; Chen, Z.; Xiao, L.; Shi, J.; Guo, X.; Wang, S.; Qu, B.; *Adv. Sci.* **2022**, *9*, 2102895. [Crossref]
164. Wang, T.; Zhou, D.; Yu, Z.; Zhou, T.; Sun, R.; Wang, Y.; Sun, X.; Wang, Y.; Shao, Y.; Song, H.; *Energy Mater. Adv.* **2023**, *4*, 0024. [Crossref]
165. Wang, C.-Y.; Liang, P.; Xie, R.-J.; Yao, Y.; Liu, P.; Yang, Y.; Hu, J.; Shao, L.; Sun, X. W.; Kang, F.; Wei, G.; *Chem. Mater.* **2020**, *32*, 7814. [Crossref]
166. S, R.; *Solid State Commun.* **2023**, *376*, 115375. [Crossref]
167. Hu, Z.; Wang, X.; Nie, K.; Zhou, R.; Dai, W.; Duan, X.; Zhang, X.; Wang, H.; Wang, L.; Mei, L.; Liu, Y.; Ma, X.; *Chem. Eng. J.* **2024**, *482*, 148829. [Crossref]
168. Zhao, S.; Xiang, J.; Fang, M.-H.; Chen, C.; Jin, M.; Zhang, N.; *Opt. Mater.* **2022**, *124*, 112052. [Crossref]
169. Li, X.; Zheng, W.; Zhang, Y.; *Nanoscale* **2022**, *14*, 12574. [Crossref]
170. Liu, N.; Zheng, W.; Sun, R.; Li, X.; Xie, X.; Wang, L.; Zhang, Y.; *Adv. Funct. Mater.* **2022**, *32*, 2110663. [Crossref]
171. Luo, J.; Li, S.; Wu, H.; Zhou, Y.; Li, Y.; Liu, J.; Li, J.; Li, K.; Yi, F.; Niu, G.; Tang, J.; *ACS Photonics* **2018**, *5*, 398. [Crossref]
172. Lei, L.-Z.; Shi, Z.-F.; Li, Y.; Ma, Z.-Z.; Zhang, F.; Xu, T.-T.; Tian, Y.-T.; Wu, D.; Li, X.-J.; Du, G.-T.; *J. Mater. Chem. C* **2018**, *6*, 7982. [Crossref]
173. Wu, C.; Du, B.; Luo, W.; Liu, Y.; Li, T.; Wang, D.; Guo, X.; Ting, H.; Fang, Z.; Wang, S.; Chen, Z.; Chen, Y.; Xiao, L.; *Adv. Opt. Mater.* **2018**, *6*, 1800811. [Crossref]
174. Sakai, N.; Haghighirad, A. A.; Filip, M. R.; Nayak, P. K.; Nayak, S.; Ramadan, A.; Wang, Z.; Giustino, F.; Snaith, H. J.; *J. Am. Chem. Soc.* **2017**, *139*, 6030. [Crossref]
175. Ghosh, S.; Paul, S.; De, S. K.; *Part. Part. Syst. Charact.* **2018**, *35*, 1800199. [Crossref]
176. Hoat, P. D.; Yun, Y.; Park, B.; Hung, P. T.; Hien, V. X.; Lee, J.-H.; Lee, S.; Heo, Y.-W.; *Scr. Mater.* **2022**, *207*, 114305. [Crossref]
177. Pan, W.; Wu, H.; Luo, J.; Deng, Z.; Ge, C.; Chen, C.; Jiang, X.; Yin, W.-J.; Niu, G.; Zhu, L.; Yin, L.; Zhou, Y.; Xie, Q.; Ke, X.; Sui, M.; Tang, J.; *Nature Photon* **2017**, *11*, 726. [Crossref]
178. Hu, Q.; Deng, Z.; Hu, M.; Zhao, A.; Zhang, Y.; Tan, Z.; Niu, G.; Wu, H.; Tang, J.; *Sci. China Chem.* **2018**, *61*, 1581. [Crossref]
179. Guo, J.; Xu, Y.; Yang, W.; Xiao, B.; Sun, Q.; Zhang, X.; Zhang, B.; Zhu, M.; Jie, W.; *ACS Appl. Mater. Interfaces* **2021**, *13*, 23928. [Crossref]
180. Wang, X.; Zhang, X.; Yan, S.; Liu, H.; Zhang, Y.; *Angew. Chem., Int. Ed.* **2022**, *61*, e202210853. [Crossref]

Submitted: January 30, 2024
Published online: May 29, 2024